Catapano *et al.*
Acta Neuropathologica Communications (2025) 13:110
https://doi.org/10.1186/s40478-025-01996-z

Acta Neuropathologica Communications

RESEARCH

Open Access

A comprehensive spatiotemporal map of dystrophin isoform expression in the developing and adult human brain

Francesco Catapano[1,2,3], Reem Alkharji[4,5], Darren Chambers[1,2,3], Simran Singh[1,2,3], Artadokht Aghaeipour[1,2], Jyoti Malhotra[6], Patrizia Ferretti[4], Rahul Phadke[1,2,3] and Francesco Muntoni[1,2*]

Abstract

Mutations in the dystrophin gene (*DMD*) cause the severe muscle-wasting disease Duchenne muscular dystrophy (DMD). Additionally, there is a high incidence of intellectual disability and neurobehavioural comorbidities in individuals with DMD. Similar behavioural abnormalities are found in *mdx* dystrophic mouse models. Unlike muscle, several dystrophin isoforms are expressed in the human brain, but a detailed map of regional and cellular localisation of dystrophin isoforms is missing. This is crucial in understanding the neuropathology of DMD individuals, and for evaluating the translatability of pre-clinical findings in DMD mouse models receiving genetic therapy interventions. Here, we provide a comprehensive dystrophin expression profile in human brains from early development to adulthood. We reveal expression of *dp427p2*, *dp427c*, *dp427m* and *dp40* isoforms in human embryonic brains, not previously reported. We also detected d*p427p2* expression and developmental regulation in human brain across the lifespan. In addition we showed by in situ hybridisation that *dp140* was greatly downregulated in adult brains. Importantly, our data also demonstrate expression of *DMD* transcripts in human motor neurons and co-expression of different dystrophin isoforms within single neurons in both developing and adult brains. Finally, we show localisation of *DMD* transcripts with *GAD1*+ GABAergic-associated transcripts in neurons including cerebellar Purkinje cells and interneurons, as well as in the majority of neocortical and hippocampal *SLC17A7*+ glutamatergic neurons, suggesting a role for dystrophin in signalling at the neuronal inhibitory and excitatory synapses.

Keywords Dystrophin, Duchenne muscular dystrophy, Intellectual disability, Human brain, GABAergic neuron, Purkinje neurons, Glutamergic neurons

*Correspondence:
Francesco Muntoni
f.muntoni@ucl.ac.uk
Full list of author information is available at the end of the article

Graphical abstract

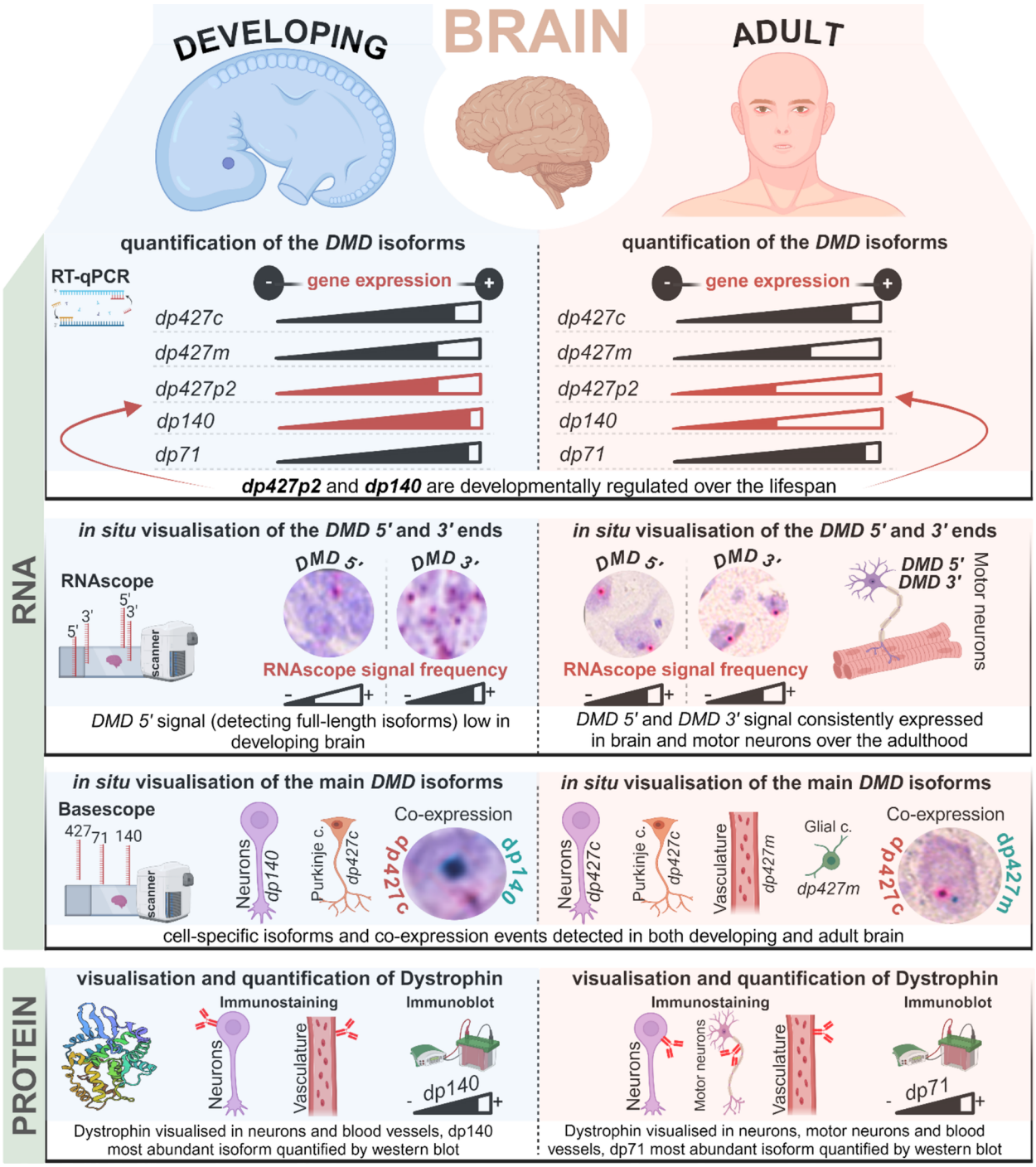

Introduction

Dystrophin (*DMD*) is the largest gene in the human genome. It consists of 79 exons located on the X chromosome and produces multiple transcripts, whose expression is regulated in a cell-tissue-specific fashion by seven promoters [1, 2]. In addition, a set of splice variants is synthesised under the regulation of multiple splicing elements and polyA sites at the *DMD* locus [2] (Fig. 1a).

Therefore, several dystrophin protein isoforms can be produced, and they are classified according to their molecular masses as full-length (*dp427m*, muscle; *dp427c*, cerebral; *dp427p*, of which there are two variants, *dp427p1* and *dp427p2*, Purkinje cells), intermediate-length (*dp260*; *dp140*; *dp116*, mainly expressed in retina, brain and Schwann cells,

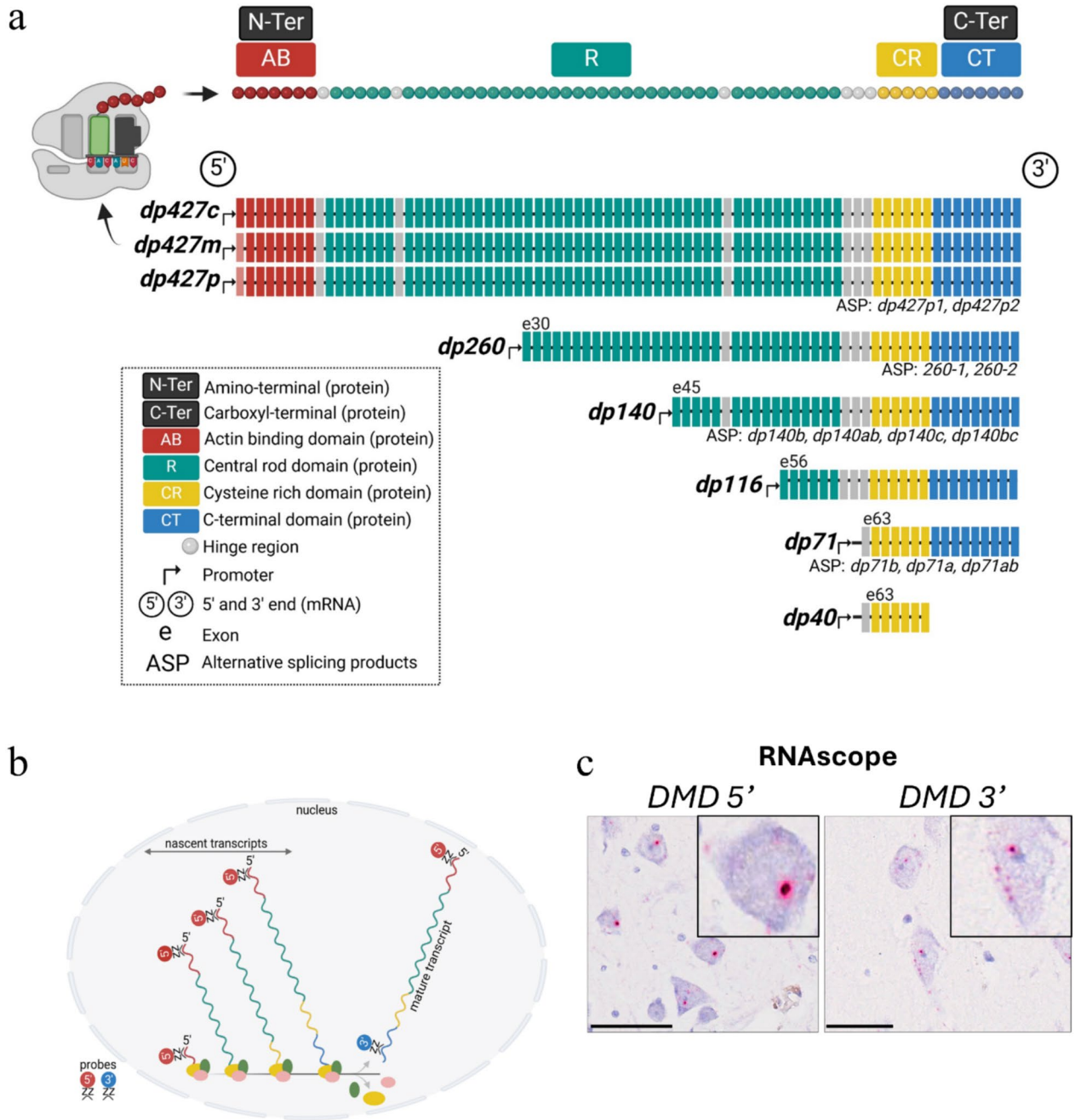

Fig. 1 Human *DMD* transcripts and RNA labelling dynamics at the 5′ and 3′ ends of the *DMD* gene protein. Isoforms derived from the *DMD* gene can be classified into full-, intermediate- and short-length according to their mass in kDa and are all expressed in the human nervous system. *DMD* exons are shown with colours matching the encoded dystrophin functional domains. ASP (alternative splicing products) are generated by alternative splicing and distinct polyA-addition signals (**a**). The *DMD* 5′ probe detects *dp427c*, *dp427m* and *dp427p* and the *DMD* 3′ probe detects all the mature *DMD* transcripts except *dp40* (**b**). Images show the variable size of the RNAscope red punctate dots detected using *DMD* 5′ and *DMD* 3′ probes (**c**). Scale bars = 50µm

respectively) and short-length (*dp71* and *dp40,* both more ubiquitously expressed) [3–5].

Loss of the muscle-specific *dp427m* isoform is the cause of the rare muscle-wasting disorder, Duchenne muscular dystrophy (DMD, OMIM #310200), that affects 1 in about 3500 live male births, and results in progressive muscle degeneration leading to premature death because of heart and pulmonary failure [6, 7]. Hence the role of dystrophin, and particularly dp427m, has been extensively investigated and is best understood in muscle [8–10].

However, it is becoming more and more recognised that DMD patients (50–70%) display central nervous system (CNS) co-morbidities, and dystrophin isoforms have been shown to be expressed in the brain [11–18].

It has been suggested that intellectual disability and behavioural comorbidities in DMD patients, including autism spectrum disorder, attention-deficit/hyperactivity disorder and epilepsy, are significantly influenced by the *DMD* mutation site, hence on which isoform expression is lost in the brain [13, 15, 16, 19, 20]. In-vivo studies in mice demonstrated that full-length *DMD* isoforms (*dp427*) are critical players in GABAergic transmission by contributing to postsynaptic gamma-aminobutyric acid A receptor (GABAARs) clustering [21].

Their deficiency in the *mdx23* mouse model, which lacks *dp427*, was associated with longitudinal changes in brain morphology, resulting in progressive cognitive impairments [22]. Similarly, a significant reduction of cortical $GABA_A$ receptors in DMD patients using position emission tomography, as compared to age-matched normal subjects, was observed and consistent with prefrontal cortex dysfunction [23].

GABAergic and glutamatergic transmission as well as behavioural and cognitive phenotypes were shown to be impaired also in the *mdx52* mouse model, deficient in both *dp140* and *dp427* [24, 25]. In accordance with the mouse phenotype, DMD patients lacking *dp427* and *dp140* were reported to present reduced cognitive function, high internalising and externalising symptoms, and increased conditioned startle response [13, 14] alongside a reduction in the grey matter and total brain volume detected by MRI [26, 27]. This reduction was greater in patients lacking both *dp427* and *dp140* than *dp427* only [26]. Finally the lack of *dp71* clearly contributes to the severity of the neural phenotype in human studies, with the mean IQ of 55 in *dp71* deficient patients [28]. A behavioural phenotype also characterises the *dp71*-null mouse model, where a selective increase in excitatory transmission at glutamatergic synapses on Purkinje neurons was observed [29].

Despite a clear correlation between deficiency of different isoforms and resulting phenotypes in the human and mouse models [30], there remain significant knowledge gaps regarding the etiopathogenesis underlying CNS co-morbidities in DMD. Current information on expression of *DMD* isoforms in the human brain is limited to the mining of transcriptomic data from publicly available databases and key limitations include lack of temporal resolution, absence of isoform and exon-specific data [12, 31, 32]. In order to understand the role of *DMD* in behaviour and cognition, and whether its expression is required for normal development, it will be crucial to generate a comprehensive map of the regional and cellular distribution of dystrophin isoforms in developing and adult human brains. It will also be important to establish whether human neural cells express single or multiple dystrophin isoforms.

Hence our aim was to systematically assess the expression and localisation of the *DMD* isoforms during development and in the adult human brain. We firstly used quantitative reverse transcription polymerase chain reaction (RT-qPCR) across multiple brain regions. We then employed 5′/3′ and isoform-specific *DMD* in situ hybridisation (ISH) probes to map *DMD* transcripts at the regional, cellular and sub-cellular levels. Using multiplex ISH probes, we studied the co-expression of *DMD* isoforms and their co-localisation with excitatory and inhibitory neurons. Specific antibodies were used to map dystrophin protein expression. Our studies provide the first comprehensive spatial and temporal expression patterns of the dystrophin isoforms of developing and adult, pathology-free human brain.

Materials and methods

Human tissues

Human tissue procedures were conducted in accordance with the regulations with informed consent in accordance with the UK Human Tissue Act 2006 for study participation under ethical approval (NRES Committee London—Fulham, UK; REC: 18/LO/0822). The human embryonic and foetal material was provided by the Joint MRC/Wellcome Trust (Grants MR/006237/1, MR/X008304/1 and 226202/Z/22/Z) Human Developmental Biology Resource (https://www.hdbr.org).

Tissue bank provided brain tissue from several donors at 17 (41 days) and 23 (56 days) Carnegie stages (CS) and 10, 14, 15, 19, and 20 post-conception weeks (PCW). Details of the subjects and samples cohorts are indicated in Supplementary Table 1.

Adult human brains: FFPE and frozen post-mortem brain specimens from four ‘non-neuromuscular’ pathology-free subjects (Supplementary Table 1) were selected and procured from the Edinburgh Brain Bank

(Ethic Ref 20/PR/0582). All subjects showed no significant abnormalities after histopathological examination of the brain. Tissue samples were obtained from the Edinburgh Brain Bank (EBB) and BRAIN UK, which is supported by Brain Tumour Research and has been established with the support of the British Neuropathological Society and the Medical Research Council [33].

Three distinct samples cohorts were available: (1) frozen and FFPE specimens from embryonic and foetal subjects; (2) five 'matching' brain areas from the same adult subjects available both frozen and FFPE and; (3) twelve remaining adult brain areas available FFPE only.

Transcript analysis

RNA isolation

According to the manufacturer's instructions, RNeasy Mini Kit (Qiagen, Cat. No. 74104) and RNeasy FFPE Kit (Qiagen, Cat. No. 73504) were used to isolate RNA from frozen and fixed sections respectively. To dissociate the sections, RLT buffer was added, and 5 mL syringes with a 25 gauge needle were used for disruption.

Total RNA concentration was measured using the NanoDrop 2000 spectrophotometer (Thermo Scientific, Cat. No. ND-2000). cDNA was generated by reverse transcription from 200 ng (frozen) and 100 ng (FFPE) of RNA using the High-Capacity RNA-to-cDNA™ Kit (Thermofisher, Cat. No. 4387406) according to the manufacturer's instructions. Next, cDNA was pre-amplified with the TaqMan™ PreAmp Master Mix (Thermofisher, Cat. No. 4391128) according to the manufacturer's instructions.

Gene expression analysis by RT-qPCR

Subsequently, *DMD* expression was detected by RT-qPCR with the TaqMan™ Fast Advanced Master Mix (Thermofisher, Cat. No. 4444557) and a set of TaqMan isoform-specific probes (Thermofisher Cat.No 4332079). A total volume of 5µL of 1:5 diluted preamplified cDNAwas used for each RT-qPCR reaction.

Relative expression was calculated by $2^{-\Delta Ct}$ formula and normalised to the brain-specific *RPL13* housekeeping gene. *RPL13* was selected as a housekeeping gene following a comparison with other *CYC1*, *GAPDH*, and *UBE2D2* genes (data not showed), demonstrating its higher consistency of expression in human brain samples, in line with previous studies. With the aim of comparing samples of different nature and therefore taking into account the variability caused by tissue fragmentation, $2^{-\Delta Ct}$ data from different sample groups were then converted to a common scale to fit within a 0–100 range, and visualised on truncated violin plots generated using the Prism 9 software (GraphPad Software LLC, Cat. No. 140000).

To mitigate the RNA fragmentation-related effects resulting from tissue fixation [34], a combined polyA/random hexamers reverse transcription and a cDNA preamplification steps were introduced for maximising the RT-qPCR sensitivity in FFPE samples [35, 36]. Despite our efforts to design probes and primers amplifying short amplicons (between 60 and 77bp) aimed at making highly sensitive RT-qPCR assays, a longer amplicon length was required for *dp427m* (88bp), *dp427p1* (81bp) and *dp40* (116bp) amplification. Consequently, when FFPE and frozen RT-qPCR results from the same area (and same subject) were compared, we detected a reduction of *dp427m* and *dp427p1* expression in the FFPEs areas. This was likely due to the larger amplicon sizes compared to the other isoforms and in particular the full-length *dp427c* (66bp). The impact of RNA fragmentation was more evident with the 116bp amplicon of *dp40* which was detected in frozen samples only. This is in line with previous reports showing that smaller amplicons produce more comparable cycle threshold (Ct) between FFPEs and frozen samples because less prone to fragmentation [35–37].

In situ hybridisation

RNAscope assays

The RNAscope in situ hybridisation (ISH) assay with its high specificity and sensitivity allows for the resolution of single mRNA transcripts which typically appear as discrete punctate/particulate foci within the cell cytoplasm and/or nuclear domains (Fig. 1c).

We assessed the prevalence and spatial distribution of *DMD* transcripts within cellular subtypes across different regions in the developing and adult human brain. Specifically, we employed a *DMD* 5′ probe targeting region (E2-E10) recognising all nascent and mature full-length transcripts (*dp427m*/*dp427c*/*dp427p*) and a *DMD* 3′ probe targeting region (E63-E75) recognising all mature dystrophin transcripts (*dp427*, *dp260*, *dp140*, *dp116*, *dp71*/*dp40*) except *dp40* (Fig. 1b). Appropriate positive and negative controls were employed in parallel to confirm RNA preservation and non-specific labeling (Fig. S7). Brain FFPE and frozen samples were pre-treated according to the existing manufacturer's instructions and incubated with probes designed by ACD Bio (Advanced Cell Diagnostics Inc., Newark, CA).

Singleplex RNAscope assays (Advanced Cell Diagnostics Inc, Cat. No. 322360) relying on RNAscope *DMD* 5′ and *DMD* 3′ probes were performed according to the manufacturer's protocol. Probes are listed in Supplementary Table 2.

Before being processed for in situ assays, selected control sections were incubated against commercially available RNAscope *UBC* (ubiquitin C) and *PPIB*

(peptidylprolyl isomerase B) probes to confirm RNA preservation. In addition, incubations with PBS/probe diluent were performed to test the extent of the background signal (negative control). Tissue staining was performed according to the manufacturer's instructions.

Basescope assays

Singleplex Basescope assays (Advanced Cell Diagnostics Inc., Cat. No. 323900) combined with a set of singleplex probes were employed to deconvolute the RNAscope signal and study the spatial expression pattern of *dp427m*, *dp427c*, *dp427p2*, *dp140*, *dp71*, and *dp40* in selected brain areas. Tests were performed according to the manufacturer's protocol (Advanced Cell Diagnostics Inc., Cat. No. 323900-USM). Probes are listed in Supplementary Table 2. A few steps were modified for embryonic/foetal tissue to avoid tissue digestion. Specifically, the target retrieval was performed for 8 min in boiling water; tissue was treated with Protease III for 30 min at 40° in high-humidity conditions. Before being processed for in situ assays, selected control sections were incubated against a commercially available Basescope *UBC* (ubiquitin C) probe to confirm RNA preservation and PBS/probe diluent to test the extent of the background signal (negative control). Tissue staining was performed according to the manufacturer's instructions.

Tissue imaging and analysis

Whole section images were acquired within 24h at 40× magnification on a NanoZoomer S60 slide scanner (Hamamtsu, Cat. No. C13210-01).

RNAscope: In situ hybridisation signal for 5′ and 3′ *DMD* transcripts was assessed by a neuropathologist in consecutive sections by carefully aligning the digital images and mapping the region of interest (ROI) for each anatomical area, primarily within morphologically identifiable neuronal elements. Scoring was based on a subjective assessment of the proportion of cells expressing transcripts within the ROI. Neurons were marked as positive irrespective of the number of transcripts (dots) expressed, and the size or staining intensity of the dots. The data was plotted on a heatmap showing the following colour code: white: unprocessed; light green = sporadic (0–5% positive cells); green = low expression (5–20% positive cells); intense green = moderate expression (20–50% positive cells); orange = frequent (50–70% positive cells); red = strong expression (> 70% positive cells); grey: undetermined.

Singleplex basescope signal semi-quantification: anatomical regions for the processed brain area were manually annotated by a neuropathologist. For each annotated region, a set of images (from three randomly selected fields of view) was exported, and the in situ signal was manually scored by three independent operators as indicated in the manufacturer guidelines. We then averaged the results obtained by the three operators and plotted the data into heatmaps. Specifically, we quantified the number of cells displaying at least one dot (positive) and calculated the P+ parameter, representing the percentage of positive cells out of the total cells. Heatmap colour code: white = unprocessed; light green = low expression; green = medium expression; orange/red = high expression; grey = undetermined.

Duplex Basescope was performed in a qualitative fashion to detect the co-expression of multiple *DMD* cellular transcripts by probes targeting the following isoforms: *dp427m* (channel 1-green), *dp427c* (channel 2-red), *dp140* (channel 1-green and channel 2-red), *dp71* (channel 2-red), *UBC* (channel 1-green) and *PPIB* (channel 2-red).

Protein analysis

Protein extraction

Protein samples were prepared on ice for extraction after adding 10 µL of extraction buffer consisting of 50 µL of protease and phosphate inhibitor mini tab (Pierce, Cat. No. A32959) to 950uL of T-PER tissue protein extraction reagent (Thermo Scientific, Cat. No. 78510) for each mg of tissue. Tissue was then homogenised using Fisher brand 850 Homogeniser (Fisher scientific, Cat. No.15–340-169) for 20 s at 10,000 and placed in an ultrasonic ice bath (Branson Ultrasonics, Cat. No. 2510-DTH) for 5 min. The homogenates were then centrifuged for 15 min at 14,000*g* at 4 °C, the supernatant was then centrifuged again at 14,000*g* at 4 °C for 5 min and kept at −70 °C. Protein extracted from the samples were quantified using RC DC Protein Assay Reagents Package (Bio-Rad Laboratories Ltd, Cat. No. 5000120).

Capillary Western immunoassay (Wes)

Simple western blot (WES, Bio-techne) was used to quantify Dystrophin levels in protein lysates from brain samples. Ab154168 (abcam) was used as the antibody with a concentration of 1:1500, which recognises all the isoform except dp40. A total of 2 µg of protein for each sample was prepared for WES analysis following protocols for the 66–440 kDa separation module (Bio-techne, Cat. No. SM-W005) and for the total protein detection module (Bio-techne, Cat. No. DM-TP01). Each dystrophin protein signal was normalised to the total protein detection signal.

Protein localisation by immunohistochemistry (IHC)

Tissue was obtained from HDBR or Brain tissue bank as formalin-fixed paraffin-embedded (FFPE) blocks or

5 µm thick paraffin sections on microscope slides. After cutting, slides were placed in an oven or hotplate for 10 min. Then, they were loaded onto the Ventana Discovery Ultra machine. First, three cycles of deparaffinisation were performed for 4 min each using EZ Prep at 65 °C. Heat Induced Epitope Retrieval (HIER) is performed using Citrate-based buffer pH 6.0 at 95 °C for three cycles (8min, 12min, 20min). Slides were washed three times using a reaction buffer (Tris-based containing ~ 2% Brij 35 and ~ 4% Acetic Acid). An amplification kit was used for primary anti-dystrophin antibodies. Two primary anti-mouse antibodies were used, one toward the C-terminus (1:150), detecting all dystrophin isoforms except dp40 (Leica Biosystems, NCL-DYS2), and the second against the rod domain (1:150) detecting longer dystrophin isoforms (NCL-DYSA, Leica Biosystems). The primary antibodies incubated for 60 min involved heating at RT. A secondary antibody was performed using OmniMap anti-Mouse HRP (Roche diagnostics, Cat. No. 760-4310), and then a Chromomere DAB kit (Biocare Medical Cat. No. ACT500) was used for nuclear staining. Finally, sections were mounted after three times washing for 2 min each and left to dry overnight.

Statistical analysis

Significant changes in transcript levels in brain tissue for dystrophin expression were assessed by one-way analysis of variance (ANOVA) to compare the differences between multiple groups (Supplementary Table 3) when 3 or more biological replicates were available. Statistical analysis was performed using the Prism 9 software (GraphPad Software LLC, Cat. No. 140000).

The p-value < 0.05 was reported as significant $^{**}p \leq 0.01$, $^{***}p \leq 0.001$ and $^{****}p \leq 0.0001$.

Results

Dystrophin isoform expression in human brains from embryo to adult

To gain insights into the regulation of dystrophin isoforms in developing and adult human brains, we first assessed their expression by RT-qPCR. Specifically, we quantified regional expression of *dp427c*, *dp427m*, *dp427p1*, *dp427p2*, *dp260-1*, *dp260-2*, *dp140*, *dp116*, *dp71/40* (sharing the first unique exon) and *dp40* isoforms in embryonic, foetal, and adult frozen and/or formalin-fixed and paraffin embedded (FFPE) post-mortem pathology-free brain samples. RT-qPCR data showing isoform brain expression from embryo to adult are summarised in Fig. 2 and S1a.

Among the full-length isoforms, the Purkinje *dp427p1* transcripts were hardly detectable or absent in developing and adult brains. *Dp427p2* showed high expression in the embryonic and foetal brain, including cerebellar and extra-cerebellar regions, but was significantly downregulated in the adult brain. The cortical *dp427c* isoform was highly expressed in the developing brain from the earliest embryonic stage studied (CS17) and its expression was maintained in most areas of adult brain, with the highest levels observed in hippocampus, amygdala, and several neocortical areas including the prefrontal cortex. Moderate to high levels of expression were also observed in the cerebellum. *Dp427m* transcripts were highly expressed throughout development and showed variable expression levels (low/moderate) in the adult brain.

The d*p260-1* splicing isoform was undetectable at all stages, whereas a low expression of *dp260-2* was detected in some developing and adult brain regions (Fig. S1a).

Among the intermediate isoforms, *dp140* was highly expressed in the embryonic and early foetal brains without regional specification, but not in the adult brain, where it became largely restricted to the cerebellum with high expression levels; lower levels of expression were detected in the dorsolateral prefrontal cortex, striate cortex and inferior frontal gyrus. Low *dp116* expression was detected in most of the frozen regions analysed.

Both short isoforms *dp71/dp40*, showed high expression levels in the embryonic and early foetal brains, and continued to remain high in the adult brain, with little regional specification.

When the 5′UTR-*dp71* and the 3′UTR-*dp40* were targeted to specifically assess *dp40* transcripts, low *dp40* expression was detected in both embryonic/foetal and adult frozen specimens, but not in adult fixed tissues (Fig. S1b), where higher RNA fragmentation occurs as explained in Materials and Methods.

In summary, all the *DMD* isoforms apart from *dp427p1* and *dp260-1* are consistently expressed in the human brain, with changes in *dp427p2* and *dp140* expression suggesting developmental regulation of these isoforms.

RNAscope in situ hybridisation assay to 5′ and 3′ regions of *DMD* mRNA allows spatial mapping of dystrophin transcripts in the developing and adult human brain

Labeling with the *DMD* 5′ probe, targeting the full-length isoforms, showed a consistent pattern across all neuronal populations in the form of a discrete, large intranuclear particulate signal, suggestive of transcriptional 'hot spots' containing multiple nascent transcripts (Fig. 1c). A few neurons also displayed smaller, punctate foci in the nucleus and/or cytoplasm. Labeling with the *DMD* 3′ probe, targeting all the isoforms apart from *dp40*, showed 1–3 large discrete intranuclear foci, and multiple smaller, mostly cytoplasmic foci, suggestive of mature transcripts (Fig. 1c).

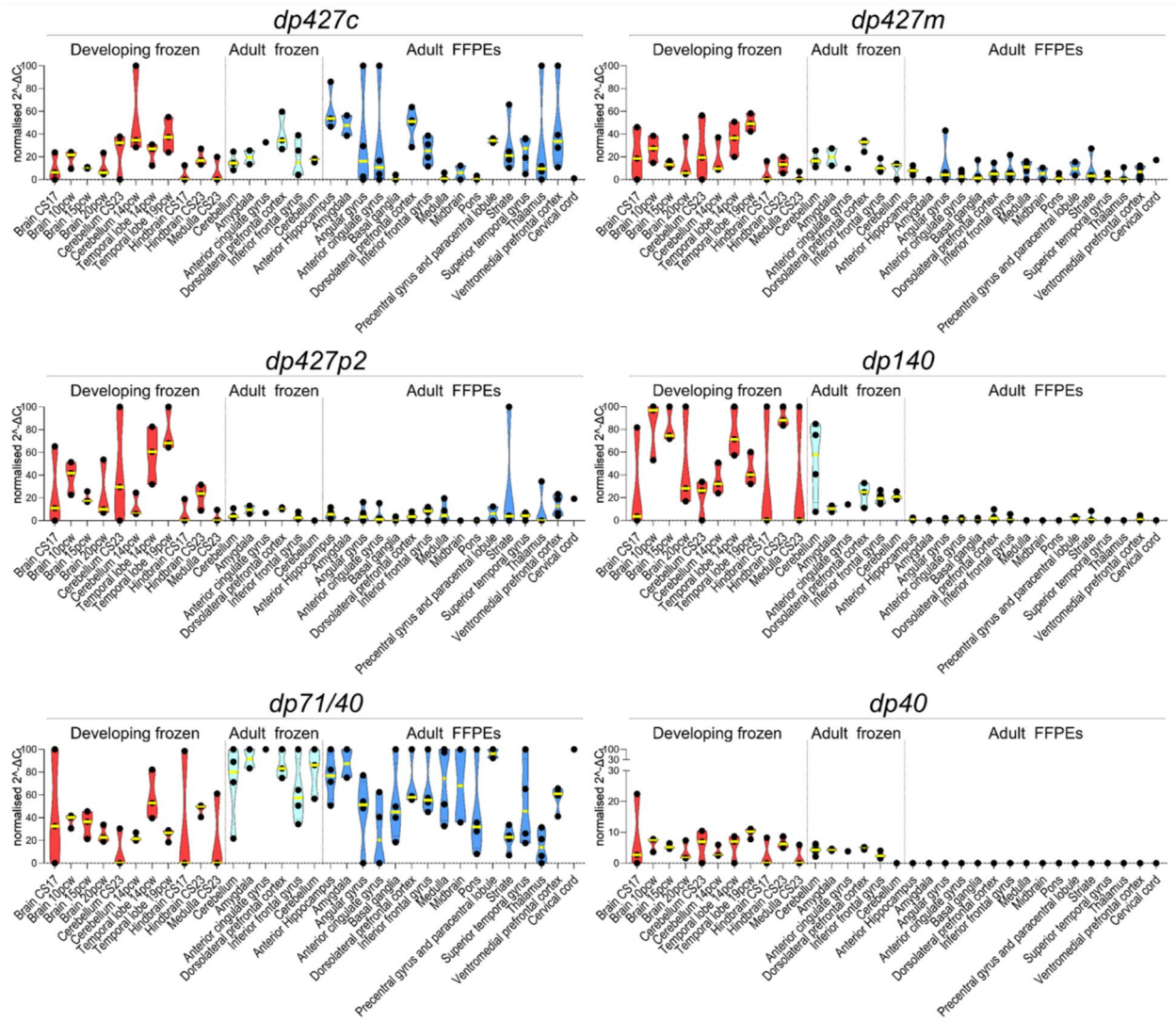

Fig. 2 Expression patterns of the main *DMD* isoforms in developing and adult brain areas assessed by RT-qPCR. Truncated violin plots showing the $2^{-\Delta Ct}$ values (converted to a 0–100 range) of the *DMD* isoforms in prenatal and adult human brains. Gene expression was normalised to the brain specific *RPL13* housekeeping gene. Yellow lines indicate the median while each black dot represents a processed sample. *Pcw* postconceptional weeks, *CS* Carnegie stage, *FFPEs* Formalin Fixed Paraffin Embedded tissue samples

Figure 3a shows a heatmap summarising the semi-quantitative values from the RNAscope signal scored by the pathologist in the adult brain, as detailed in the Materials and Methods section.

To identify changes in *DMD* localisation with development, section from embryos and foetuses at developmental stages between CS17, CS23 and PCW19 were hybridised with either the *DMD* 3′ or the *DMD* 5′ probe (Figs. 4, 5, 6 and Fig. S2).

In the brain region studied in CS17 embryos, with the exception of the trigeminal ganglion, more extensive and ubiquitous labeling was observed with the *DMD* 3′ probe than with the *DMD* 5′ probe, suggesting higher expression of shorter-length *DMD* isoforms than long ones (Fig. 4). The *DMD* 3′ signal was particularly abundant across the neuroepithelium of telencephalon, hippocampus, cerebellum, pons and medulla, and was the only signal detected in the optic vesicle (Fig. 4 and Fig. S2a). *DMD* 5′ signal was localised to neuroepithelial cells in pons and medulla, suggesting expression of full-length *DMD* isoforms in these areas. The hybridisation pattern observed suggests that at CS17 *DMD* is predominantly expressed in neural progenitor cells and early migratory neurons. The CS17 skeletal muscles expressed both *DMD*

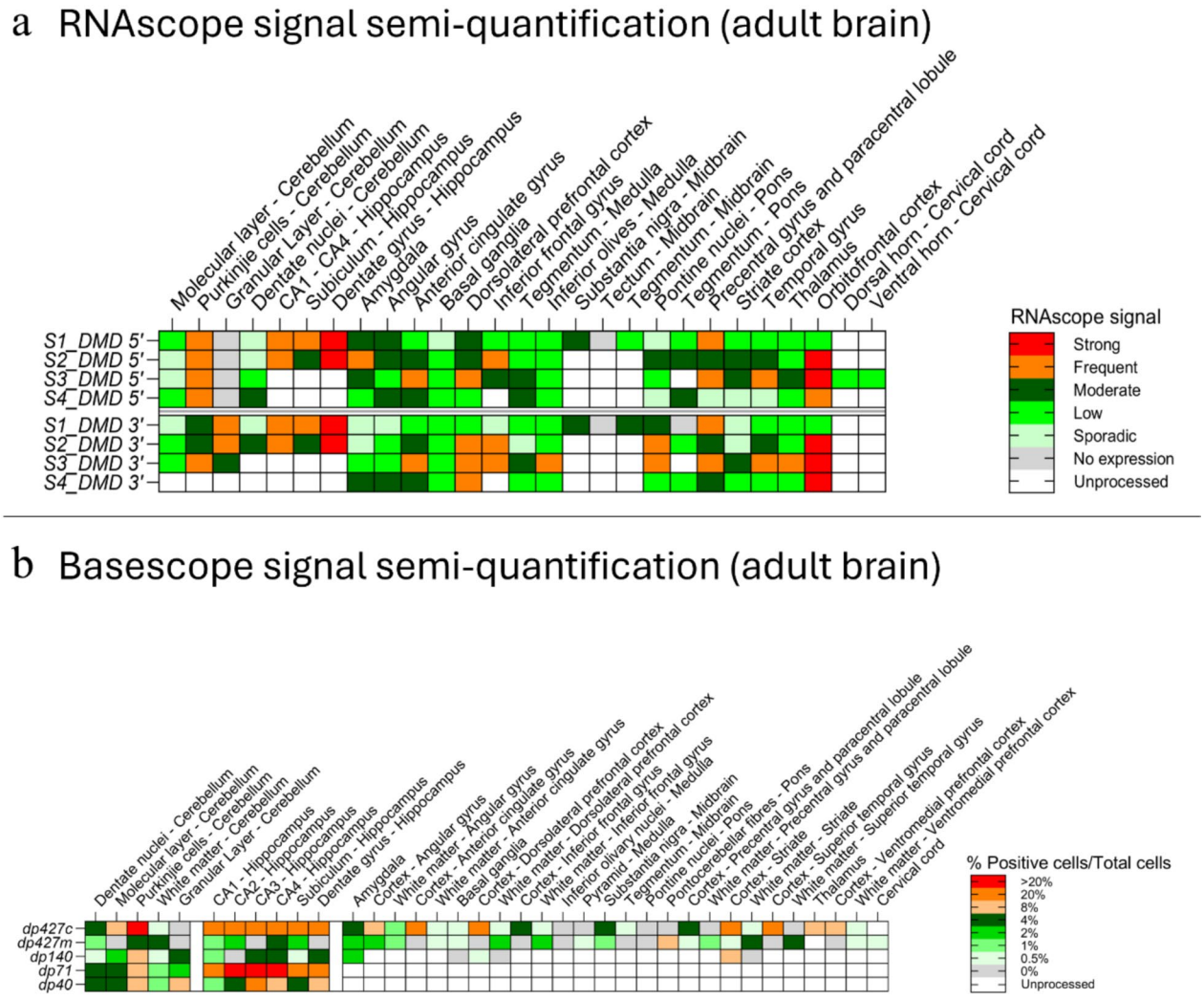

Fig. 3 In situ hybridisation in the human brain. Heatmap representing the *DMD* 5′ and *DMD* 3′ RNAscope signal scores in each adult ROIs (**a**). Heatmap representing the singleplex Basescope P+ (% Positive cells/total cells) across different adult brain areas (**b**). Colour code: white: unprocessed; light green: low expression; green: moderate expression; orange/red: high expression; grey: undetermined; S1-4: subjects processed for each developmental stage

5′ and *DMD* 3′ transcripts, providing a positive control for both probes (Fig. 4).

At the late embryonic stage CS23, *DMD* 3′ labeled transcripts were widely distributed in the telencephalon, hippocampus and cerebellum as well as in amygdala, cerebral cortex, basal ganglia, medulla and retina (Figs. 5, S2b and S4a). *DMD* 5′ labeled full-length transcripts were more widely expressed at CS23 than at CS17 in all regions studied apart from the hippocampus (Figs. 5 and S2b), but the *DMD* 3′signal remained the more robust one. The CS23 muscle continued to show positive signal with both probes (Fig. S2b).

At foetal stages, PCW14 and PCW19, *DMD* 3′ labeled transcripts were widely distributed in the hippocampus and cerebellum as well as in other brain regions (Figs. 6, S2c-d and S4a). At PCW14, *DMD* 5′ labeled transcripts were detected in the cerebellum, but not in cortical areas such as the cingulate gyrus and paracentral lobe (Figs. S2c and S4a). By PCW19, the *DMD* 5′ signal had become more widely expressed and, unlike at earlier stages, was detected also in the hippocampus, especially in the granule cells of the dentate gyrus and in the CA1 area, and in the subiculum, as well as in the cerebellum, where it was particularly striking in Purkinje cells and deep nuclei, with large puncta observed (Figs. 6 and S2d).

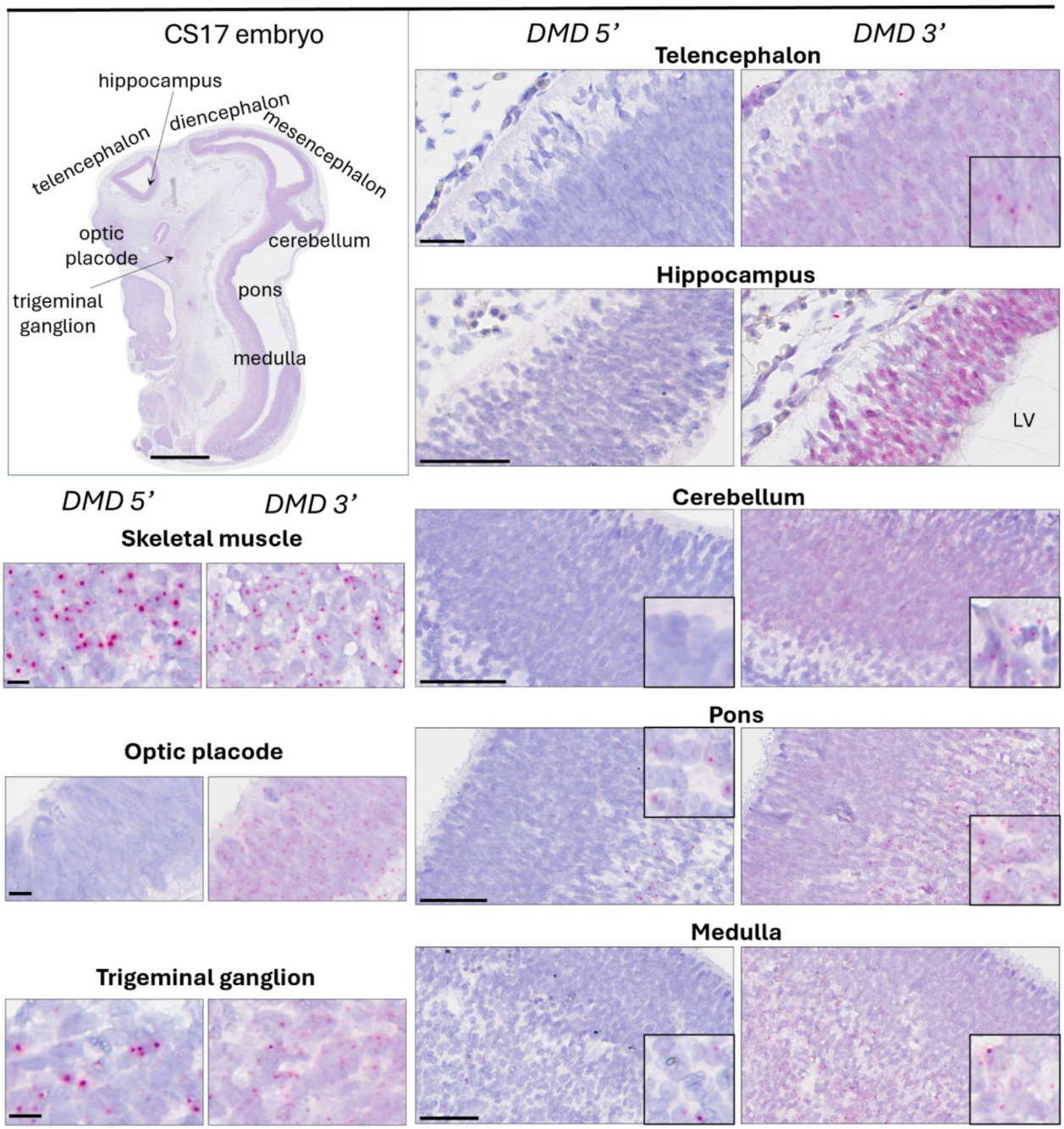

Fig. 4 *DMD* transcript detection by RNAscope in embryonic human brain at Carnegie stage 17 (CS17). Top left image shows a low magnification of a CS17 embryo sagittal section. Individual plates show representative images of brain sections from the regions indicated in the CS17 embryo hybridised either with the *DMD* 5′ or *DMD* 3′ probe. Note extensive *DMD* 3′ signal in all brain regions, whereas the *DMD5′* signal is either not detectable or detected only in a few cells, with the exception of the trigeminal ganglion where several positive cells are observed. As positive control, representative images of FFPE muscle sections hybridised either with the *DMD* 5′ or the *DMD* 3′ probe are shown; note extensive signal with both probes (red dots). Inserts show representative puncta at a higher magnification. Scale bars are: embryo = 1 mm; images on left column = 10 µm; telencephalon = 25 µm; all other images = 50 µm

In the adult cerebellar cortex, *DMD* 5′ and *DMD* 3′ labeled transcripts were noted in the molecular and Purkinje cell layers (Figs. 7b, S3a and S4b), whereas only *DMD* 3′ labeled transcripts were seen in the granule cell layer (Figs. 7d, S3a and S4b), suggesting abundant expression of shorter mature transcripts in these cells (*dp140*/*dp71*). Both *DMD* 5′ and *DMD* 3′ labeled transcript were seen in the dentate nucleus (Fig. 7c, f). In the

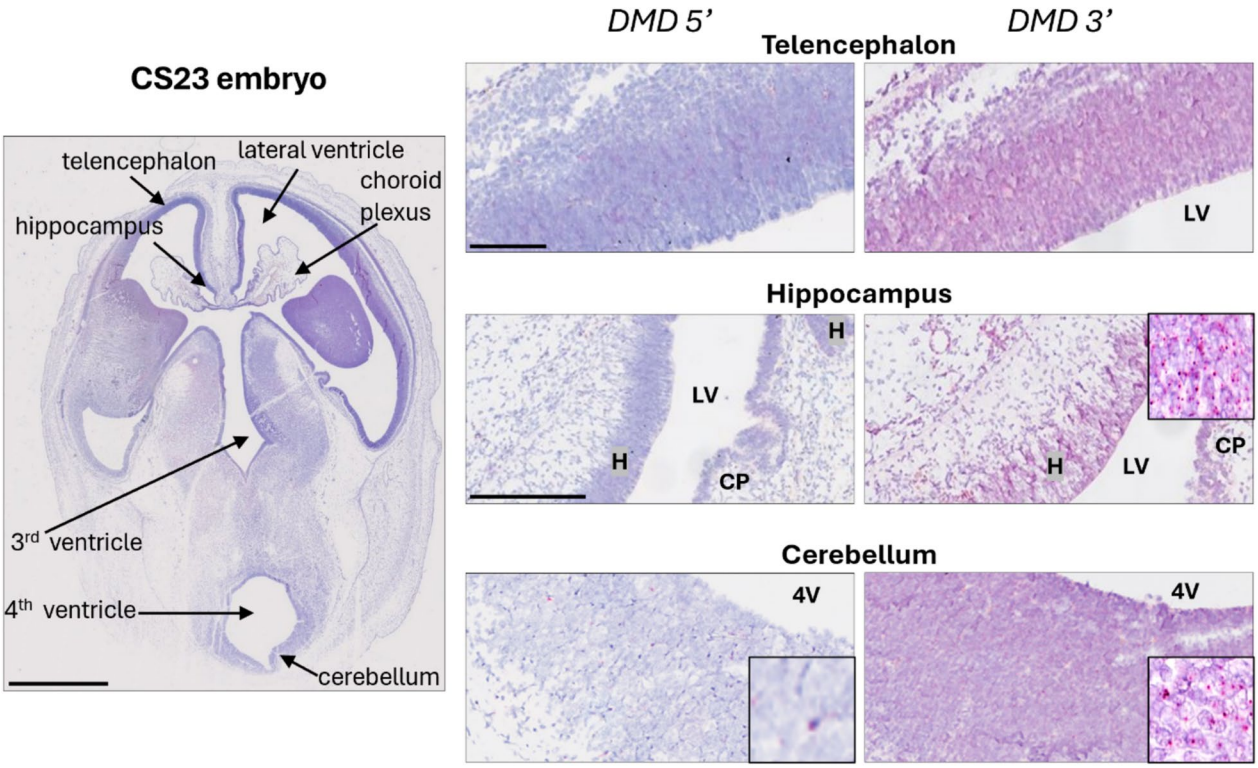

Fig. 5 *DMD* transcript detection by RNAscope in embryonic human brain at Carnegie stage 23 (CS23). The left image shows a low magnification of a CS23 embryonic brain coronal section highlighting main structures at this stage of development. Right panels show representative images of telencephalon, hippocampus and cerebellum hybridised either with the *DMD* 5′ or *DMD* 3′ probe. Note extensive *DMD* 3′ signal in all brain regions with representative puncta shown at higher magnification in the inserts; the *DMD* 5′ signal is very sparse (telencephalon and cerebellum) or absent (hippocampus). *CP* choroid plexus, *H* hippocampus, *LV* lateral ventricle, *4V* 4th ventricle. Scale bars are: CS23 embryo = 2 mm telencephalon and cerebellum = 100 µm; hippocampus = 250 µm

adult brain *DMD* transcripts were abundant in the hippocampus proper CA1-CA3, CA4/hilar region and the dentate fascia (Figs. 7g–m and S3a). While both *DMD* 5′ and 3′ transcripts were localised within the amygdala, subregional (nucleus-wise) specification could not be ascertained due to suboptimal orientation of the blocks (Fig. S3a). High expression was detected in the prefrontal cortices and inferior frontal gyrus (Fig. 8).

Moreover, *DMD* 5′ and *DMD* 3′ labeled transcripts were widely expressed across several neocortical regions: primary motor cortex, dorsolateral and ventromedial prefrontal cortex, inferior frontal gyrus, superior temporal gyrus, angular gyrus, calcarine/striate cortex and anterior cingulate gyrus (Fig. 8a–i and S3a). The expression pattern was similar across these regions with pan-cortical localisation of transcripts. Within the cortices, most transcripts were neuronal, including majority of pyramidal cells (Figs. 8b, c and S3a) and a small proportion of the 5′ transcripts localised to oligodendroglia-like cells in the cortex and white matter (Fig. S3a). Both *DMD* 5′ and *DMD* 3′ labeled transcripts were localised to the upper motor neurons, the giant pyramidal cells of Betz (Fig. 8h, i). *DMD* 3′ and *DMD* 5′ labeled transcripts were observed in several other brain areas such as Pons, Medulla and hypoglossal nerves (Fig. 8m–v).

Basescope *DMD* isoform-specific, singleplex and multiplex in situ hybridisation assays reveal isoform diversity and coexpression within neuronal, glial and vascular domains across key brain regions

Singleplex Basescope: As RNAscope did not provide information on expression and localisation of specific *DMD* isoforms, we used singleplex Basescope assays to localise dystrophin isoforms, *dp427c*, *dp427m*, *dp140*, *dp71*, and *dp40*. We could not study *dp427p2* due to lack of specificity of the labelling probe. Expression of these isoforms was semi-quantified in adult brains and shown as a heatmap (Fig. 3b), and examples of cellular localisation are shown in Figs. 9 and S3b. In the adult brain, *dp427c* transcript was widely expressed across all neocortical regions (Fig. 9w), and also in the hippocampus (Fig. 9r-s), amygdala (Fig. S3b) and cerebellum (Figs. 9c,

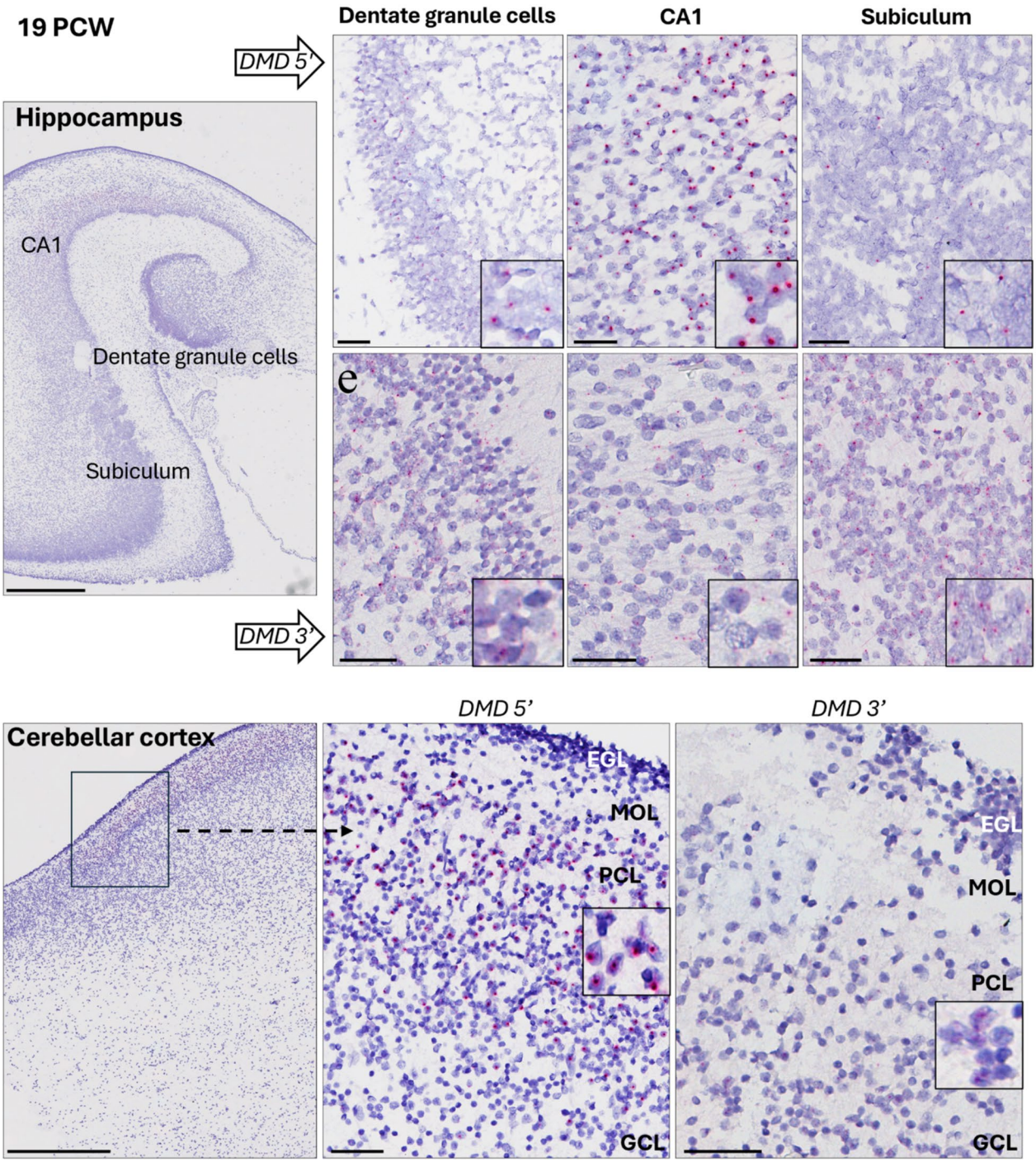

Fig. 6 *DMD* transcript detection by RNAscope in a 19 weeks post-conception (PCW19) foetal human brain. Left images show a low magnification of PCW19 hippocampus and cerebellum with localisation of regions shown on the left indicated. Individual plates on the right show representative sections of hippocampus and cerebellum hybridised either with the *DMD* 5′ or *DMD* 3′ probe. Signal from both probes is detected in the dentate granule cells, CA1 and subiculum of the hippocampus, as well as in all cerebellar layers: external granular layer (EGL), molecular layer (MOL), Purkinje cell layer (PCL) and granule cell layer (GCL). Some representative puncta are shown at higher magnification in the inserts. Scale bars are: low magnification hippocampus and cerebellar cortex = 1 mm and = 500 µm, respectively; all other images = 40 µm

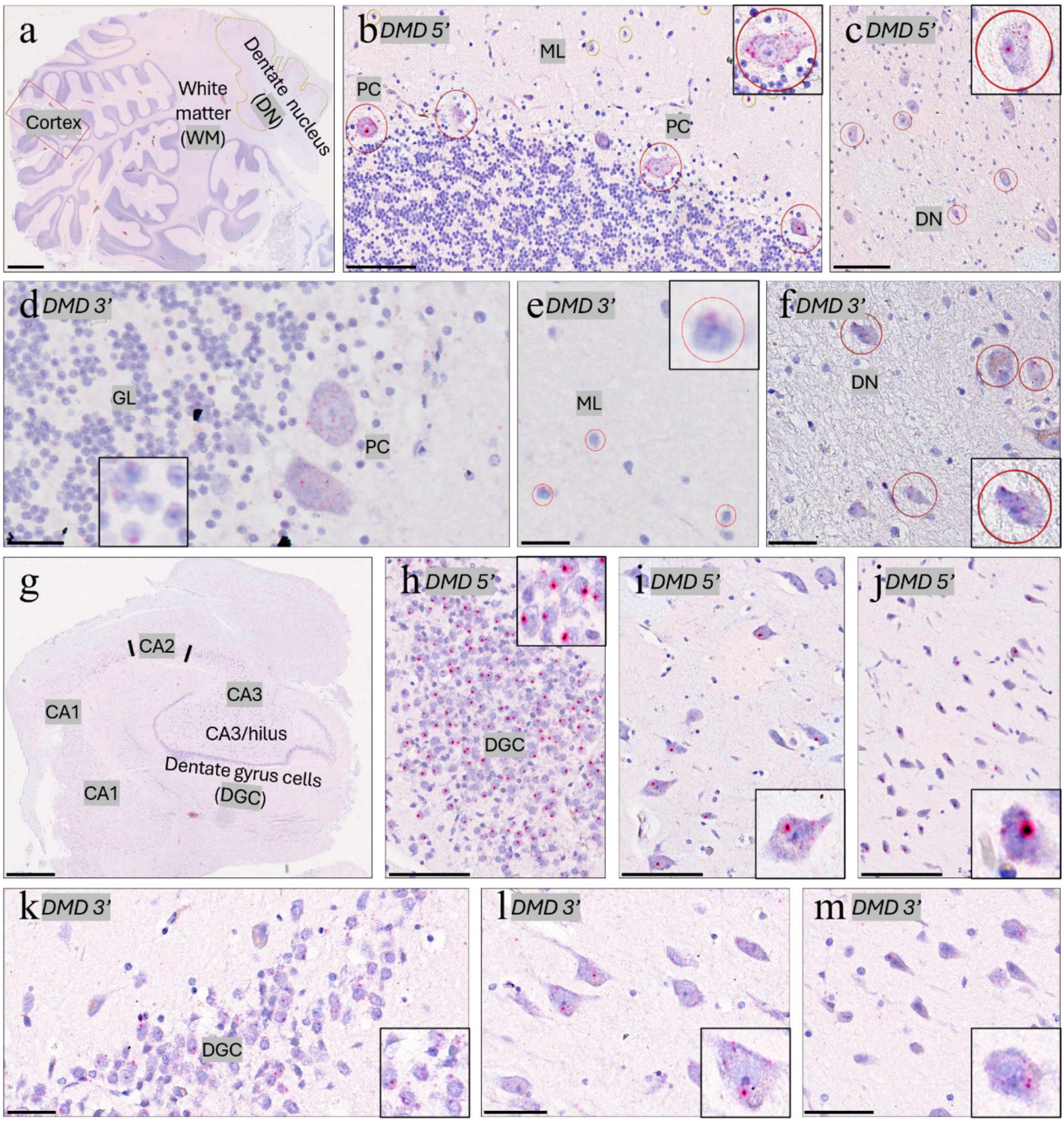

Fig. 7 Expression of *DMD* 5′ and 3′ labeled transcripts in the adult cerebellum (**a**–**f**) and hippocampus (**g-m**). Low power overview of the cerebellum (**a**). In the molecular layer, scattered small cells, likely interneurons (**e**, red circles) express 3′ labeled transcripts. The large Purkinje cells (red circles) abundantly express 5′ (**b**), and 3′ (**d**) labeled transcripts. The granule cell layer preferentially expresses 3′ labeled transcripts (**b**, **d**). Neurons in the dentate nucleus (red circles) also express both 5′ (**c**) and 3′ (**f**) labeled transcripts. Low power overview of the hippocampus (**g**). There is frequent expression *DMD* transcripts in the granule cells of the dentate gyrus [5′ (**h**), 3′ (**k**)], CA3/hilus [**i** (5′), **l** (3′) and CA1 [**j** (5′), **m** (3′)]. *WM* white matter, *ML* molecular layer, *PC* Purkinje cell layer, *GL* granule cell layer, *DN* dentate nucleus, *DGC* dentate granule cells. Scale bars are: g = 1 mm; a = 2.5 mm; c, h and i = 100 µm; l and m = 50 µm; all other images = 25 µm

g, j and Sb3). *Dp427m* was consistently expressed within the leptomeningeal (Fig. 9l) and cortical blood vessels (Fig. S3b) containing a muscular coat (most likely in the smooth muscle cells).

Dp140 transcripts were expressed in the dorsolateral and ventromedial prefrontal cortices and the striate cortex (Fig. S3b). *Dp71* was detected in the ventromedial orbitofrontal cortex with transcripts identified in pyramidal cells.

In the adult hippocampus, the granule cells in the dentate gyrus showed moderate to frequent expression of *dp427c* (Figs. 9r and S3b), *dp140* and *dp71* (Figs. 9u and S3b) and low levels of *dp427m* and *dp40* transcripts. The hilum/CA4, CA1-CA3 and subiculum showed moderate expression of *dp427c* and *dp71* (Figs. 9s–v and S3b), and low level of *dp427m* transcripts.

The amygdala showed low levels of *dp427c* and *dp140* expression (Fig. S3b). Very few neurons expressed *dp427m* (Fig. S3b). Sparse *dp427c* transcripts were noted in the basal ganglia. Few oligodendroglial cells expressed *dp427m* in the white matter (Fig. S3b). The thalamus showed moderate expression of *dp427c* (Fig. S3b). *Dp427m* signal was noted mostly in oligodendroglia, and rarely in neurons.

In the midbrain, dystrophin transcripts were mainly present in the substantia nigra pigmented neurons, specifically, *dp427c,* with occasional neurons expressing *dp427m*. The dorsal midbrain and the midbrain tegmentum showed occasional *dp427c* and *dp427m* in the Edinger Westphal nuclei (Fig. S3b), oculomotor nerve nuclei and the mid-line raphe neurons.

The pontine tegmentum, including the pigmented neurons of the locus coeruli, the periventricular grey, the midline raphe nuclei and the pontine reticular formation showed modest expression of *dp427c* and *dp140* transcripts. Similarly in the basis pontis, there was moderate expression of *dp427c*, *dp427m, dp140* and *dp71* transcripts in the pontine nuclei. *Dp427m* expression was also noted in the oligodendroglial cells within the white matter tracts (corticopontine, corticospinal and pontocerebellar fibres) (Fig. S3b).

In the medulla, sparse *dp427c* transcripts were localised to the medullary tegmentum (hypoglossal nuclei and reticular formation) and the inferior olivary nucleus. *Dp427m* was expressed in oligodendroglial cells in the pyramidal tracts and the emerging rootlets of the vagus nerve.

The adult cerebellum showed few *dp40* and *dp71* (Fig. 9h) transcripts expressed within the molecular layer (likely in interneurons), Purkinje cells, dentate nucleus (Fig. S3b) and granule cells. *Dp71* transcripts were also seen within the parenchymal capillary walls (Fig. 9p) and the pia-glial membrane (glia limitans), but not within the leptomeningeal blood vessels. In the cerebellum, *dp140* transcripts were detected in a moderate number of granule cell layer (Fig. 9f). A small number of molecular layer neurons, Purkinje cells and dentate neurons also expressed *dp140* transcripts. Moderate numbers of Purkinje cells and neurons in the dentate nucleus and few interneurons in the molecular layer expressed *dp427c* (Fig. 9c, j). In contrast, there was no *dp427c* signal in the granular cell layer. *Dp427m* expression was restricted to sparse basket cells within the Purkinje cell layer.

Duplex Basescope: In addition, duplex Basescope with *dp427m*/*dp427c*, *dp140*/*dp427c*, *dp427m*/*dp140* and *dp427m*/*dp71* probes was used to further assess isoform localisation in the adult brain, and establish whether more than one dystrophin isoform may be expressed in the same cell (Figs. 10 and S5).

In the adult brain, neuronal *dp140/dp427c* co-expression was seen in the, hippocampus, pons, striate cortex and dorsolateral prefrontal cortex while rare neuronal events were noted in pyramidal cells across all hippocampal subsectors and in the amygdala (Fig. 10b). Co-expression of the two full length *dp427c*/*dp427m* isoforms was seen in one of the midbrain's raphe neurons (Fig. 10b). Unexpectedly, moderate *dp427m* signal was

(See figure on next page.)

Fig. 8 Expression of *DMD* 5′ and 3′ labeled transcripts in the adult dorsolateral prefrontal cortex (**a**–**g**), primary motor cortex (**h**, **i**), brain stem (**j**–**l**), pons (**m-o**) and medulla (**p**-**v**). Low power overview of the hexalaminar dorsolateral prefrontal cortex shows expression of 5′ and 3′ labeled transcripts in all layers (red circles). Higher magnification depicts examples of 5′ transcripts expressed in pyramidal cells of layers III (**b**), V (**c**), and polymorphic neurons in layer VI (**d**), and 3′ labeled transcripts expressed in pyramidal cells of layers III (**f**) and V (**g**). Within layer V of the precentral gyrus (primary motor cortex) the large pyramidal Betz cells (upper motor neurons) express both 5′ (**h**) and 3′ (**i**) labeled transcripts. A small cell, likely interneuron, expresses 3′ labeled transcript (**i**, black arrow). Overview of the mid brain substantia nigra, pars compacta (**j**). Higher magnification view within the region of interest (**j**, red rectangle) shows expression of both 5′ (**k**) and 3′ (**l**) labeled transcripts in the large dopaminergic pigmented neurons. Low power overview of the pons (**m**). Higher magnification shows neurons in the pontine nuclei expressing both 5′ (**n**) and 3′ (**o**) labeled transcripts. Low power view of the medulla sectioned at the level of the inferior olivary nucleus. Neurons within the hypoglossal nerve nucleus preferentially express 3′ labeled transcripts (**s**) over 5′ labeled transcripts (**q**). Neurons within the inferior olivary nucleus express both 5′ (**r**) and 3′ (**t**) labeled transcripts. Scale bars are: m and p = 2.5 mm; a and **e** = 250 µm; u = 100 µm; all other images = 50 µm

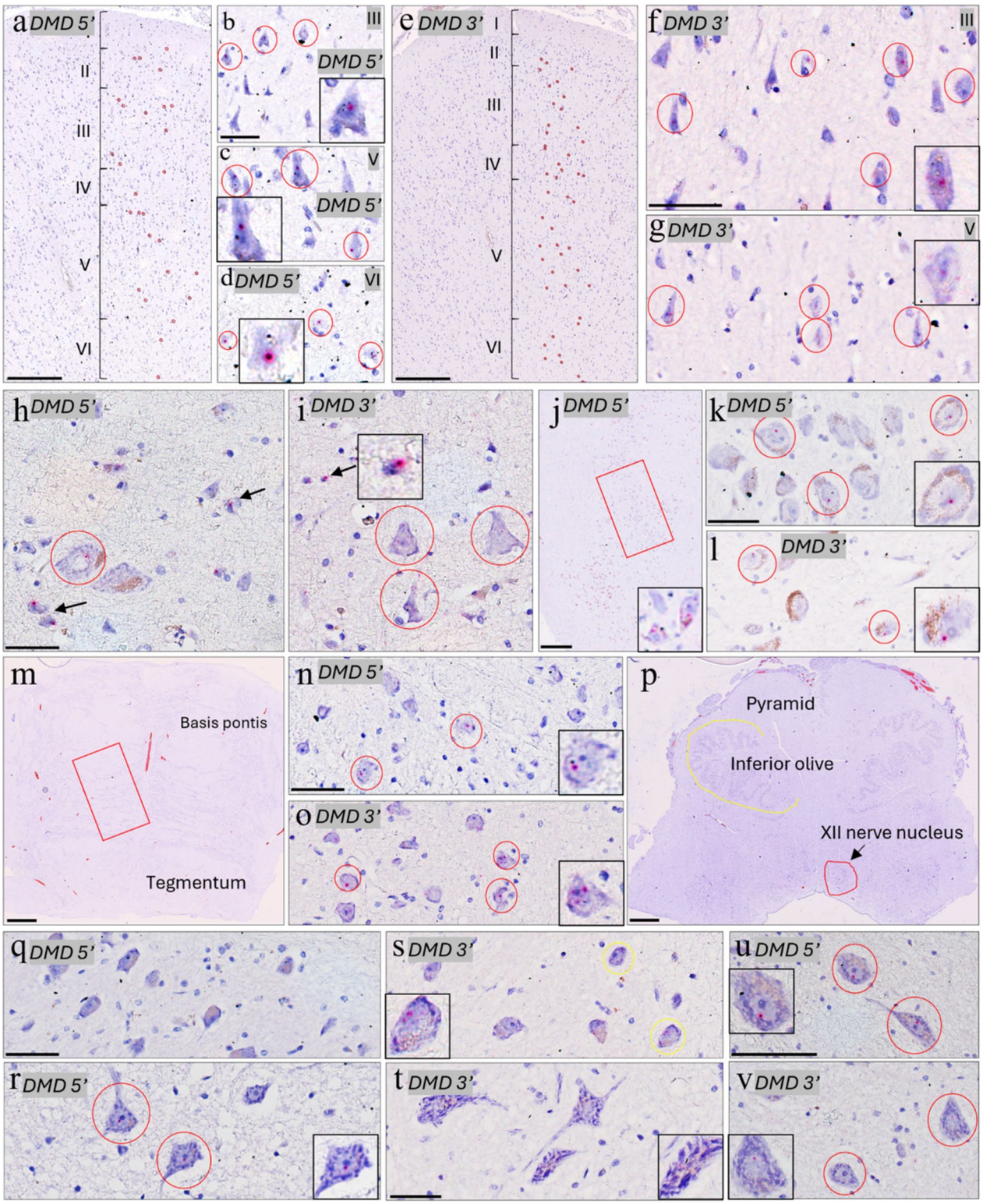

Fig. 8 (See legend on previous page.)

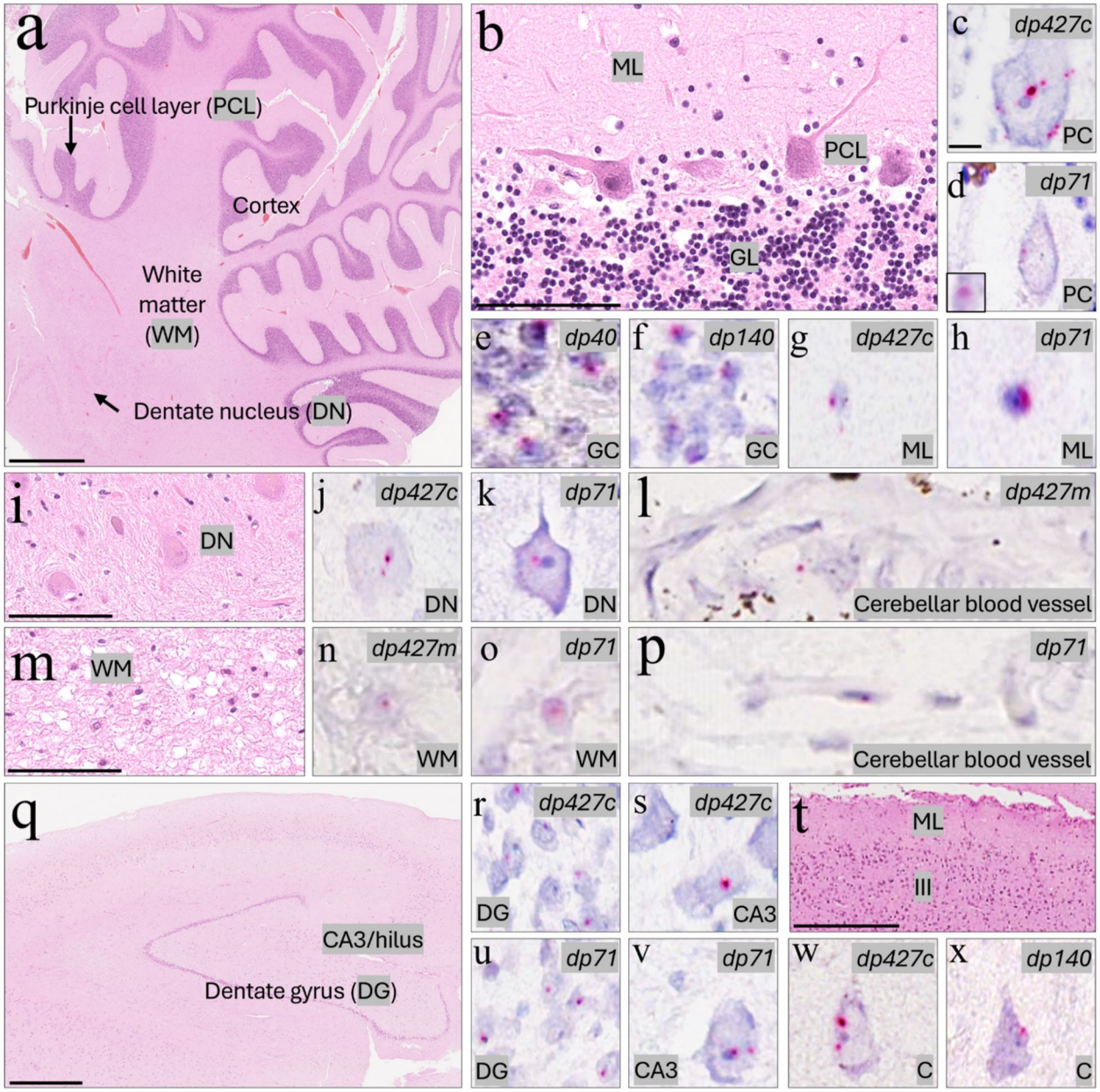

Fig. 9 Expression of *DMD* isoform-specific transcripts in the adult cerebellum (**a**–**p**), hippocampus (**q**–**s**, **u**, **v**), and primary visual (striate) cortex (**t**–**x**). Low power overview of the cerebellum (**a**). Three layered cerebellar cortex (**b**). Purkinje cells expressing *dp427c* (**c**) and *dp71* (**d**) transcripts. Granule cells expressing *dp40* (**e**) and *dp140* (**f**) transcripts. Scattered small cells, likely interneurons within the molecular layer expressing *dp427c* (**g**) and dp71 (**h**) transcripts. Neurons within the dentate nucleus (**i**) expressing *dp427c* (**j**) and *dp71* (**k**) and in the white matter (**m**) expressing *dp427m* (**n**) and *dp71* (**o**). A leptomeningeal blood vessel expressing mural *dp427m* transcripts (**l**). A parenchymal capillary-sized small blood vessel shows *dp71* expression in its wall (**p**). Low power overview of the hippocampus (**q**). Dentate granule cells express *dp427c* (**r**) and *dp71* (**u**) transcripts. Pyramidal cells in CA3 express *dp427c* (s) and *dp71* (v) transcripts. Overview of the striate cortex (**t**). Cortical pyramidal cells within layer III expressing *dp427c* (**w** and *dp140* (**x**) transcripts. *ML* molecular layer, *PCL* Purkinje cell layer, *PC* Purkinje cell, *GL* granule cell layer, *GC* granule cells, *DN* dentate nucleus, *DG* dentate gyrus. Scale bars are: a = 2.5 mm; q = 1 mm; t = 0.5 mm; b, i, m = 100 µm; all other images = 10 µm

noted in oligodendrocytes, both within the cerebellar white matter, the cortex and the underlying white matter across all neocortical areas (Figs. 10b) and S5a).

Due to the limited number of prenatal sections available, we elected to study CS17, CS23 and 14 pcw sections for duplex BaseScope with the *dp140/dp427c* isoforms as they were the most relevant neuronal

transcripts previously detected by RT-qPCR. In these sections, we detected a robust *dp140* expression (Fig. 10a), consistent with the RT-qPCR data and in line with previous literature findings, indicating *dp140* abundancy during the early stages of life. At embryonic CS stages 17 and 23 *Dp140* transcripts were most abundant and widely expressed in the developing CNS, including the telencephalic cortical plate, dorsal hippocampus, thalamic, mesencephalic, cerebellar and brain stem neuroepithelia. *Dp140* transcripts were noted in the subventricular germinal neuroepithelium as well as the early migrating neurons. Co-expression of *dp140/dp427c* isoforms was also detected in the CS17 embryonic pons and during the foetal 14pcw stage in cerebellum, hippocampus and cingulate gyrus (Fig. 10a). *Dp427c* transcripts were also ubiquitous, but fewer compared to *Dp140*, except in the mesencephalon where they were seen in abundance.

At 14 pcw, the developing cerebellum showed preponderance of *Dp427c* transcripts in the Purkinje cell zone, whereas *Dp140* transcripts were more frequent in the external granule cell layer and the dentate nucleus. Expression of *Dp71* and *Dp40* was not assessed in the embryonic and foetal samples.

Altogether, results from singleplex and duplex Basescope assays confirmed that *dp427c* is abundantly expressed in neurons across all brain regions from early development to adulthood. *Dp427m* is expressed mainly in the leptomeningeal blood vessels, and small number of oligodendroglial cells and neurons (Fig. S5a–c). *Dp140* is highly expressed in embryonic and foetal brains and continues to be expressed at low to moderate levels in the adult forebrain, cerebellum and the brain stem. *Dp71* is widely expressed in neurons, as well as the parenchymal microvasculature and the glia limitans. The adult human hippocampus (dentate granule cells), cerebellum (Purkinje cells) and pons (neurons in the pontine nuclei) show the greatest diversity of dystrophin isoform expression.

DMD expression in excitatory and inhibitory neurons

Due to constraints in multiplex immunohistochemistry in FFPE tissues, we used duplex RNAscope comprising dual labeling of *DMD* 5′ and *DMD* 3′ probes with *GAD1* as a proxy for GABAergic inhibitory neurons and *SLC17A7* as a proxy for glutamatergic excitatory neurons. In the 14 pcw cerebellum, the migrating Purkinje cells coexpressed *GAD1* and *DMD* 3′ transcripts (Figs. 11a, b). In contrast, in the granular cell layer, few cells coexpressed *SLC17A7* and *DMD* 3′ transcripts (Fig. 11c, d). In the adult cerebellum, this distinction was even more pronounced, with coexpression of *DMD* 5′ and *GAD1* transcripts in the molecular layer interneurons (Fig. 11k), Purkinje cells (Fig. 11e) and majority of cells in the dentate nucleus (Fig. 11f), whereas *DMD* 3′ and *SLC17A7* transcripts were coexpressed mainly in the granule cells (Fig. 11i) and a small number of neurons in the dentate nucleus.

In the adult hippocampus, an overwhelming majority of dentate neurons and pyramidal cells (CA1-CA3) coexpressed *DMD3′* and *SLC17A7* transcripts (Fig. 11l, n), and a small number of cells, most likely interneurons coexpressed *DMD* 3′ and *GAD1* transcripts (Fig. 11m). A similar pattern was evident in the neocortical areas examined, with most pyramidal cells coexpressing *DMD* 3′ and *SLC17A7* transcripts (Fig. S6b–f). Notably, there was no evidence of labeling in the subcortical and/or deep white matter with any of the probes above.

Immunohistochemical localisation of the dystrophin protein in the developing and adult human brain

In order to establish whether there was concordance of dystrophin transcript and protein expression, developing and adult brains were immunostained with the antibodies to dystrophin, DYS2, that reacts with the C-terminus, hence detects all isoforms apart from dp40, as well as DYSA. The latter antibody recognises an undisclosed epitope in the rod domain, but previously characterised in mice, and shown to detect both full-length (dp427) and shorter (dp71) isoforms of the dystrophin protein [30].

At stage CS17, DYS2 reactivity was detected in the cerebellum, pons, and medulla, whereas DYSA staining was negative (Fig. 12a), indicating that the longer isoforms are not present, or their expression is below the sensitivity of the method, at this early developmental stage. Similarly, only DYS2 reactivity was observed in the CS23 cerebellum (Fig. 12b), whereas weak DYSA reactivity was detected in the CS23 trigeminal ganglia (Fig. 12b). At the

(See figure on next page.)

Fig. 10 Detection of co-expressed *DMD* isoforms in developing and adult human brain areas by duplex Basescope. Representative images of developing brain samples hybridised with the *dp140* (green) and *dp427c* (red) probes. Note some cells express both isoforms (**a**). Representative images of adult brain samples hybridised with four different probe combinations: *dp427m*(green)/*dp427c*(red); *dp427m*(green)/*dp140*(red); *dp427m* (green)/*dp71*(red); *dp140* (green)/*dp427c*(red) (**b**). Red and green arrows indicate RNA transcripts (dots) co-expressed in the same cell. The top left inset shows the co-expression events at a higher magnification. *bv* blood vessels, *Pcw* postconceptional weeks, *CS* Carnegie stage; Hippocampus *CA* Cornu Ammonis. Scale bars = 10 µm

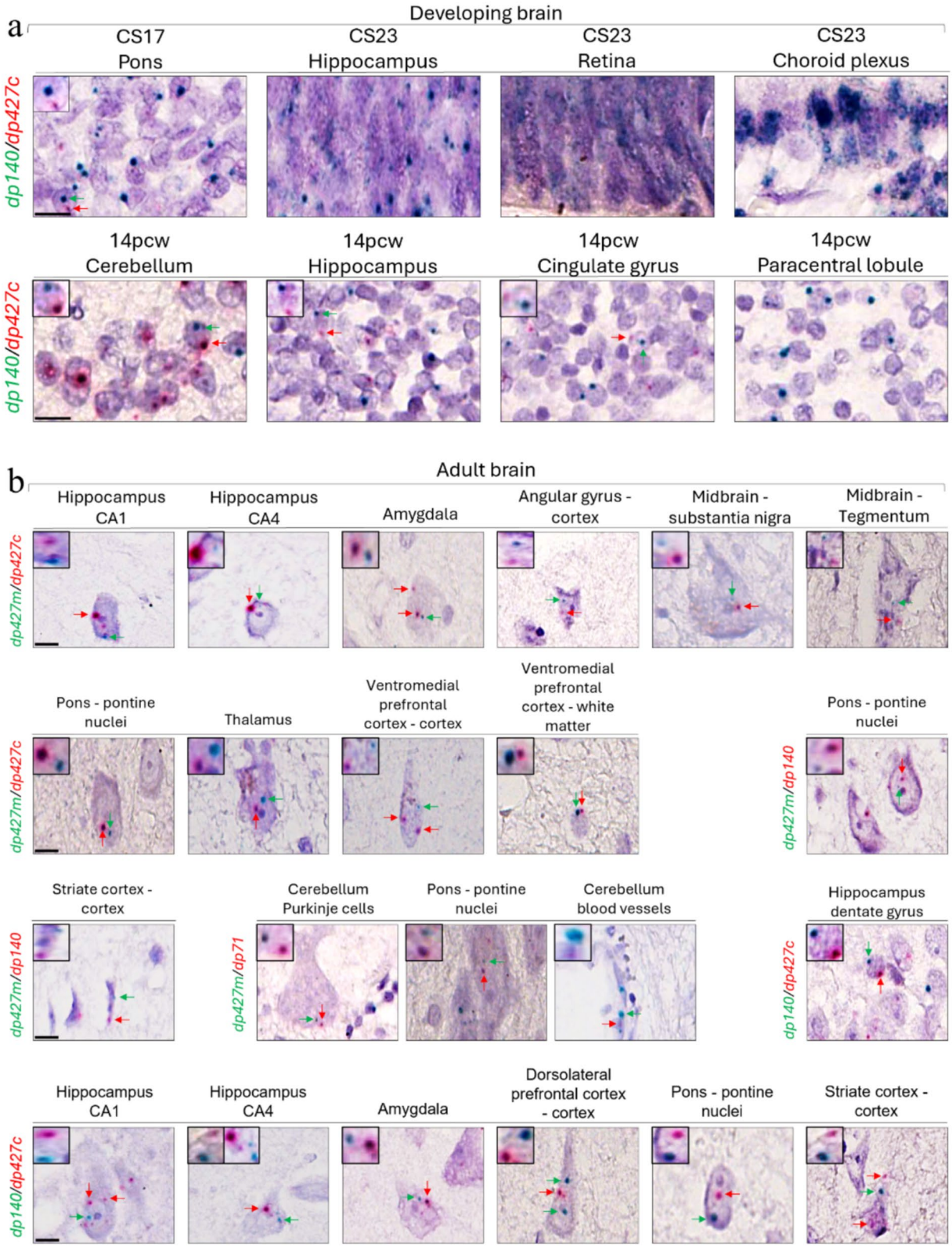

Fig. 10 (See legend on previous page.)

foetal stage examined, 14pcw, both cerebellum and hippocampus showed some DYS2 staining but very weak DYSA reactivity, suggesting predominant expression of shorter isoforms (Fig. 12c).

In contrast, in adult brains DYSA strongly stained several neuronal cell types. Dystrophin expression across all neocortical regions was pan-cortical (Fig. 12d), sometimes with accentuated labelling in layer II and layer V/VI. The expression pattern was more readily discernible within the pyramidal cells, partly owing to the size of these neurons. Moderate to strong labelling was observed within the neuronal cell body, with accentuated punctate distribution along the cell surface and the dendritic trees, whereas the axons were negative. There was strong dystrophin expression in the upper motor neurons, so-called giant pyramidal cells of Betz, within the precentral gyrus (Fig. 12e).

In the hippocampus, dystrophin immunoreactivity was noted within the dentate granule cells, hilar/CA4 region, Ammon's horn (CA1–CA3) and the subiculum, restricted to the neuronal somata and their dendritic trees (Fig. 12d). Within the amygdaloid complex the presence of large amounts of lipofuscin pigment confounded ascertainment of dystrophin signal within the neurons (Fig. 12d).

In the cerebellum, Purkinje cells displayed a distinct punctate labelling pattern at the surface of the cell bodies and their dendritic arbour (Fig. 12d). Small neurons within the molecular layers were also labelled as were a significant proportion of the cells in the granular cell layer. In the midbrain, weak labelling was seen in the oculomotor nerve nuclei. The presence of abundant neuromelanin in the substantia nigra pigmented neurones confounded the assessment for dystrophin expression. Strong labelling were noted within the neurons (pontine nuclei) and the surrounding neuropil in the pontine base. In the medulla, the neuropil within the inferior olivary nuclear ribbon showed a strong DYSA signal. Unexpectedly, there was strong labelling of the axons within the vagus and hypoglossal nerves. The respective nuclei displayed dystrophin expression in the surrounding neuropil. The anterior horn cells in the spinal cord showed robust dystrophin expression within the neuronal cell bodies and dendrites (Fig. 12e). Of note, these motor neurons expressed both 5′ and 3′ labeled *DMD tr*anscripts (Fig. 12e, f).

Dystrophin and *DMD* expression within the non-neural cell types

In the CS23 choroid plexus, only RNAscope *DMD* 3′ labeling was seen (Fig. 13a). In contrast, both probes labelled the choroid plexus at 14pcw, but antibody reactivity was clearly detected only with DYS2 (Fig. 13b). At CS23, only the RNAscope *DMD* 3′ signal was noted in the blood vessel wall with corresponding exclusive DYS2 immunoreactivity. At 14 pcw stage, the vessel walls showed expression of both RNAscope *DMD* 5′ and *DMD* 3′ labeled transcripts, and immunoreactivity for both DYSA and DYS2 antibodies (Fig. 13e). In the adult brain, the leptomeningeal, penetrating arteries and arterioles showed predominant expression of RNAscope *DMD* 5′ labeled transcripts localised to the vascular smooth muscle cells (Fig. 13f, g). At the isoform level, *dp427m* was consistently expressed in the smooth muscle coats of the leptomeningeal and cortical penetrating arteries and arterioles (Fig. 13f, g). *Dp71* transcripts were noted in the parenchymal capillary walls and the glia limitans (Fig. 13h, i).

Developmental regulation of dystrophin protein isoforms in the human brain assessed by capillary western blot

As immunohistochemical cellular localisation of different dystrophin isoforms in FFPE sections was hindered by the lack of isoform-specific dystrophin antibodies, analysis of protein isoform expression and semi-quantification was carried out by WES using a C-terminal antibody (Ab154168) in protein extracts from frozen developing and adult brains (Fig. 14). Protein peaks with the molecular weights of dp427, dp140, and dp71 were detected in all the brain areas from developing and adult samples, while dp116 was detected in 3 out of 5 adult brain areas (cerebellum, amygdala, and dorsolateral prefrontal cortex).

During development, apart from CS17, dp140 was the predominant isoform detected in all brain regions assayed with an average relative protein concentration (RPC) of 0.58, followed by dp71 (average RPC = 0.25), and dp427 appeared to be the less expressed isoform

(See figure on next page.)

Fig. 11 Detection of *DMD* isoforms, GABAergic and glutamatergic neurons in developing and adult human brain areas by duplex RNAscope. Representative image of experiments performed in 14pcw cerebellum (**a**–**d**). Representative images of the results from the adult samples (**e**–**n**). Green dots indicate RNAscope *DMD* 5′ and *DMD* 3′ transcripts. Red signal indicates *GAD1* (GABAergic) or *SLC17A7* (glutamatergic) transcripts. Black arrows indicate migrating Purkinje neurons (**a**) external granular layer (**c**) *GAD1*- or low *GAD1*+ Purkinje neurons (**e**, **g**). The green arrow shows sporadic *DMD* 3′ signal in **d**. Red arrows indicate *GAD1*+ Purkinje neurons (**e**, **g**) and *GAD1*+ dentate neurons (**f**, **h**) in the cerebellum. Scale bars are: a, e, l = 50 µm; all other images = 10 µm

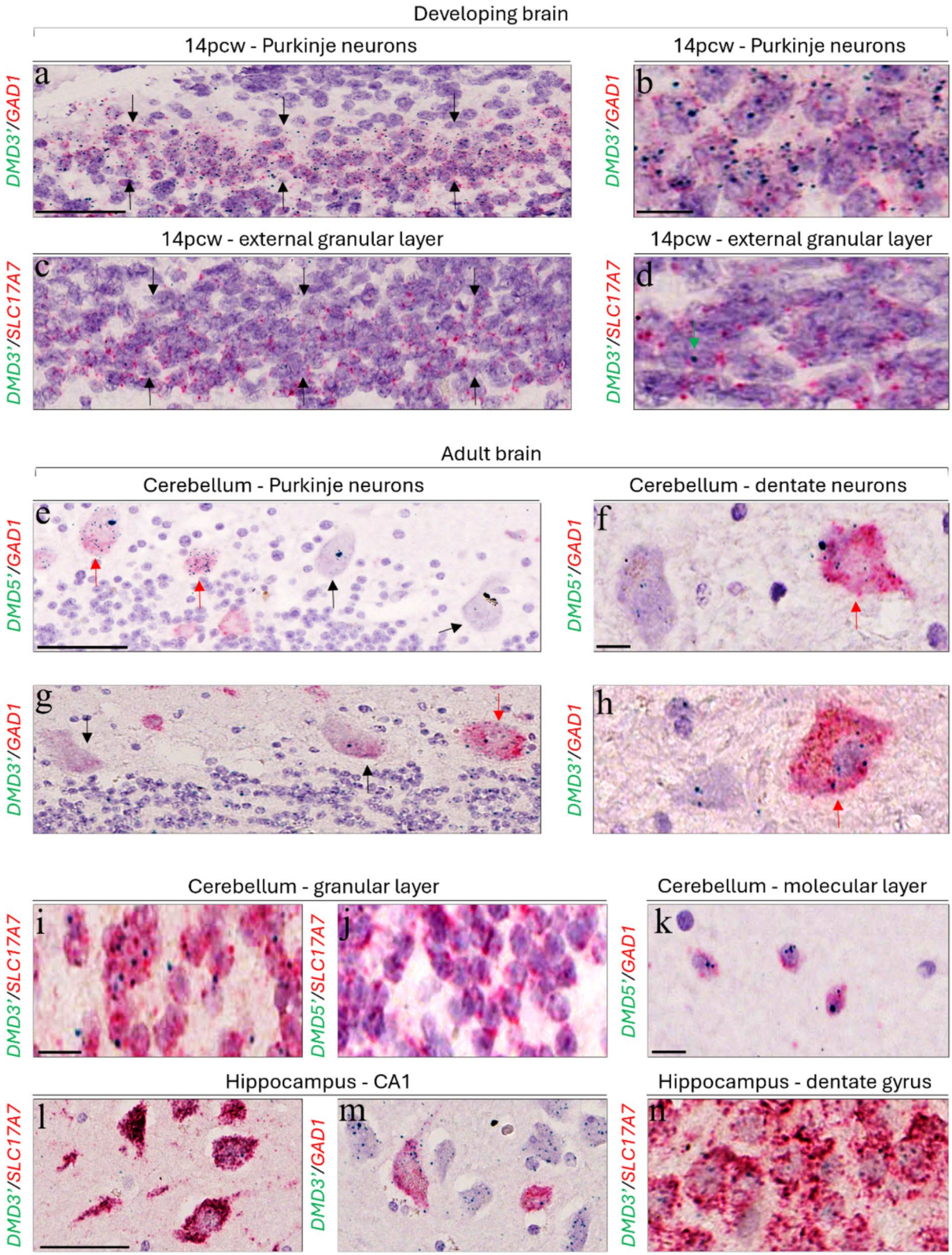

Fig. 11 (See legend on previous page.)

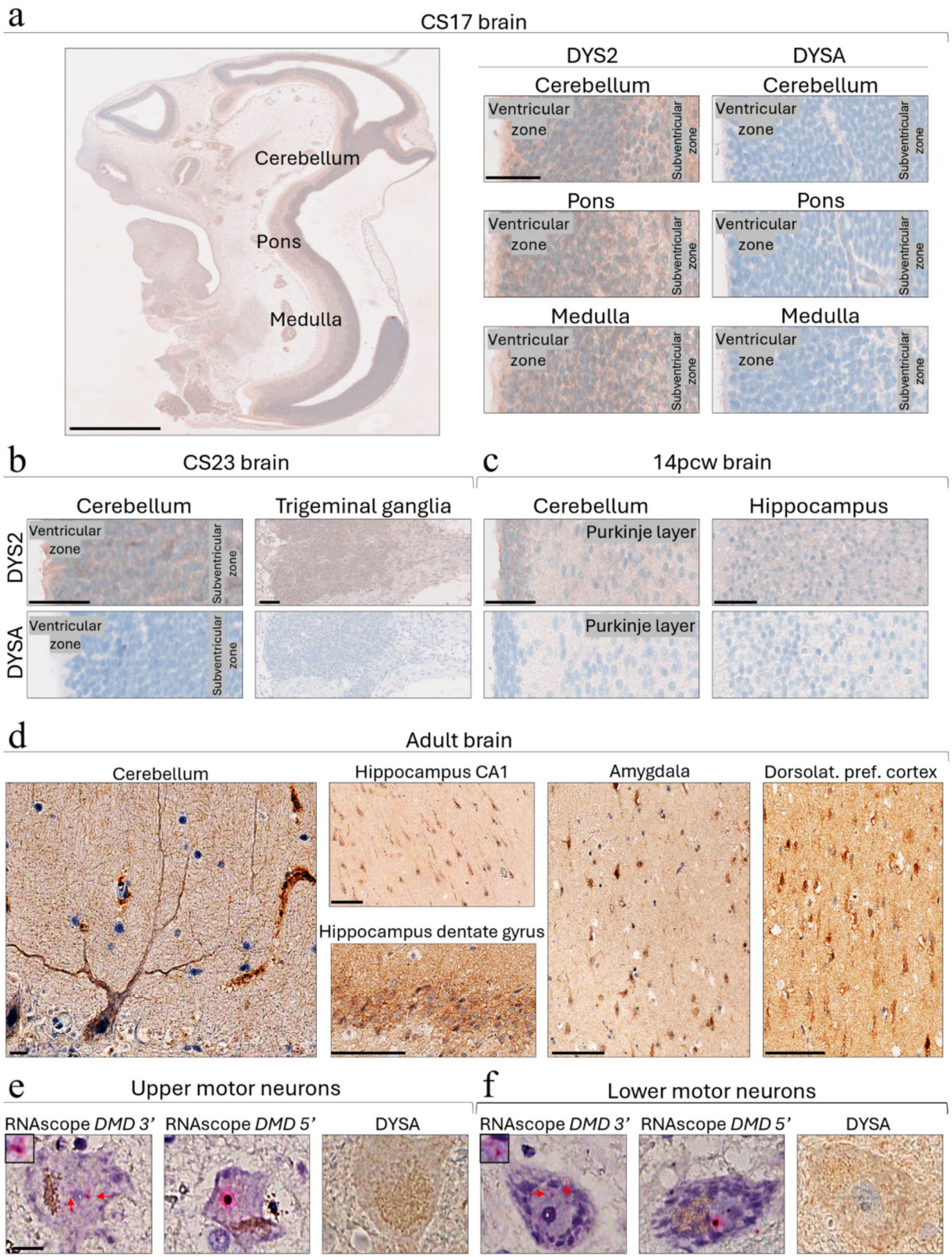

Fig. 12 Dystrophin detection by immunohistochemistry in developing and adult brain regions. Developing brains stained either with the monoclonal antibody DYSA (dystrophin N-Terminus) or DYS2 (dystrophin C-Terminus) (**a**–**c**). Adult brain sections stained with DYSA (**d**). Adult upper and lower motor neurons stained with DYSA and RNAscope *DMD* 5′ and *DMD* 3′ probes (**e**–**f**). *Pcw* postconceptional weeks, *CS* Carnegie stage. Scale bars are: a = 1 mm (overview) and 50 µm; d = 100 µm; b and c = 50 µm all other images = 10 µm

(average RPC = 0.11), with the exception of CS17 brain (RPC = 0.6). In contrast, dp71 was the predominant isoform in all adult brain regions, and dp140, though expressed throughout was greatly reduced as compared to developing brains, as particularly evident in the cerebellum (RPC = 0.73 in developing cerebellum versus 0.07 in adult). Dp116 was selectively expressed in adult cerebellum (RPC = 0.24), amygdala (average RPC = 0.32) and dorsolateral prefrontal cortex (RPC = 0.28), but not in cingulate and frontal gyrus nor in embryonic/foetal samples. Although this technique did not allow us to pinpoint which of the long isoforms was expressed, it showed that dp427 was expressed, though to different extents, in all adult brain regions examined.

Together, good concordance between protein and transcript isoform expression was observed, with changes in dp140 and dp71 protein expression from developing to adult brain closely mirroring transcript changes, with the former being higher prenatally and the latter postnatally. However a degree of discordance between the levels of some protein and transcript was noted especially in some adult brain areas, potentially due to non-specific tissue contamination in the frozen specimen processed for WES.

Discussion

This study provides a comprehensive analysis of isoform-specific dystrophin expression in developing and adult pathology-free human brains combining a variety of quantitative methods (RT-qPCR and immunoblot), in situ hybridisation and immunohistochemistry techniques that deliver, for the first time, a comprehensive neuroanatomical, cellular and sub-cellular context to the dystrophin expression profile.

Our RNAscope studies, that allow for spatial localisation of the *DMD* transcripts, provide novel information on the complexities of *DMD* expression in the human brain. The *DMD* 5′ signal appeared as both large juxtanuclear/intranuclear dots, suggestive of transcriptional 'hotspots' containing multiple full-length nascent and mature transcripts, whereas the *DMD* 3′ signal consisted of multiple small cytoplasmic dots, indicating the presence of nascent and mature transcripts as previously described in the dog by Hildyard et al. [38].

Our results show that in the human brain the *DMD* 3′ signal was robust throughout the embryonic and foetal developmental stages, whereas the *DMD* 5′ signal increased from early to late development. This is consistent with the work by Doorenweerd et al., but it should be noted that the study did not cover embryonic stages of development, nor localised the transcripts at the cellular level [12]. Here we show that *DMD* transcripts were already abundant at an early developmental stage, CS17 (6 weeks of gestation) and mainly localised to neuroepithelial cells. This is consistent with *DMD* expression in the developing dog brain [38], suggesting an important and conserved role of *DMD* in early neural development. Significantly, the dystrophin interacting protein, dystroglycan, has been suggested to play a role in the maturation of the mouse perinatal neural stem cell niche, partly via regulation of Notch signalling, an important pathway in neural development [39, 40]; therefore, it is tempting to speculate that dystrophin may modulate Notch signalling in the human neuroepithelium.

Furthermore, the human hippocampus and cerebellar Purkinje cell layer also showed high expression of *DMD* transcripts. The complete absence of *DMD* 5′ signal in the granule cells of the developing and adult cerebellum was striking, supporting a cell-specific specialised role for the shorter isoforms, as suggested in dog cerebellum [38, 41]. The granular layer of the cerebellum appears to express mainly shorter isoforms, as in the dog, whereas both short and long isoforms are detected in the Purkinje cells. Altogether, our RNAscope data showed that *DMD* transcripts are ubiquitously expressed in the developing and adult human brain.

When isoform-specific *DMD* transcripts were spatially mapped by Basescope and quantified by RT-qPCR, *dp427c* showed consistent high expression across most regions in the developing and the adult brain. This is in contrast to the study by Doorenweerd et al. showing low-level expression across human brain development [12]. Also in contrast to previous findings reporting no expression of *dp427p* in the developing

(See figure on next page.)

Fig. 13 Dystrophin protein and transcript expression in brain vasculature. Embryonic and foetal choroid plexus and blood vessels stained with DYSA and DYS2 antibodies and hybridised with the RNAscope *DMD* 5′ and *DMD* 3′ probes (**a**–**e**). Adult blood vessels stained with DYSA antibody and processed for RNAscope or Duplex Basescope (**f**–**i**). Note positive signal detected with duplex Basescope (*Dp427m*-green/*Dp71*-red), RNAscope *DMD* 5′ *and DMD* 3′ probes, and the DYSA antibody within the tunica media of a medium-sized leptomeningeal artery (**f**) and in a cortical penetrating arteriole (**g**) in the ventromedial prefrontal/orbitofrontal cortex. Note also expression of the *Dp71* transcript and DYSA immunoreactivity in the cerebellar cortical parenchymal capillary (**h**) and cerebellar pial–glial membrane (glia limitans) at the cortical surface (**i**). Each red arrow indicates RNAscope or duplex Basescope (*dp71*) signal (red dots) while green arrows indicate duplex Basescope (*dp427m*) signal (green dots). Scale bars are: f, g, h, i = 25 µm; all other images = 10 µm

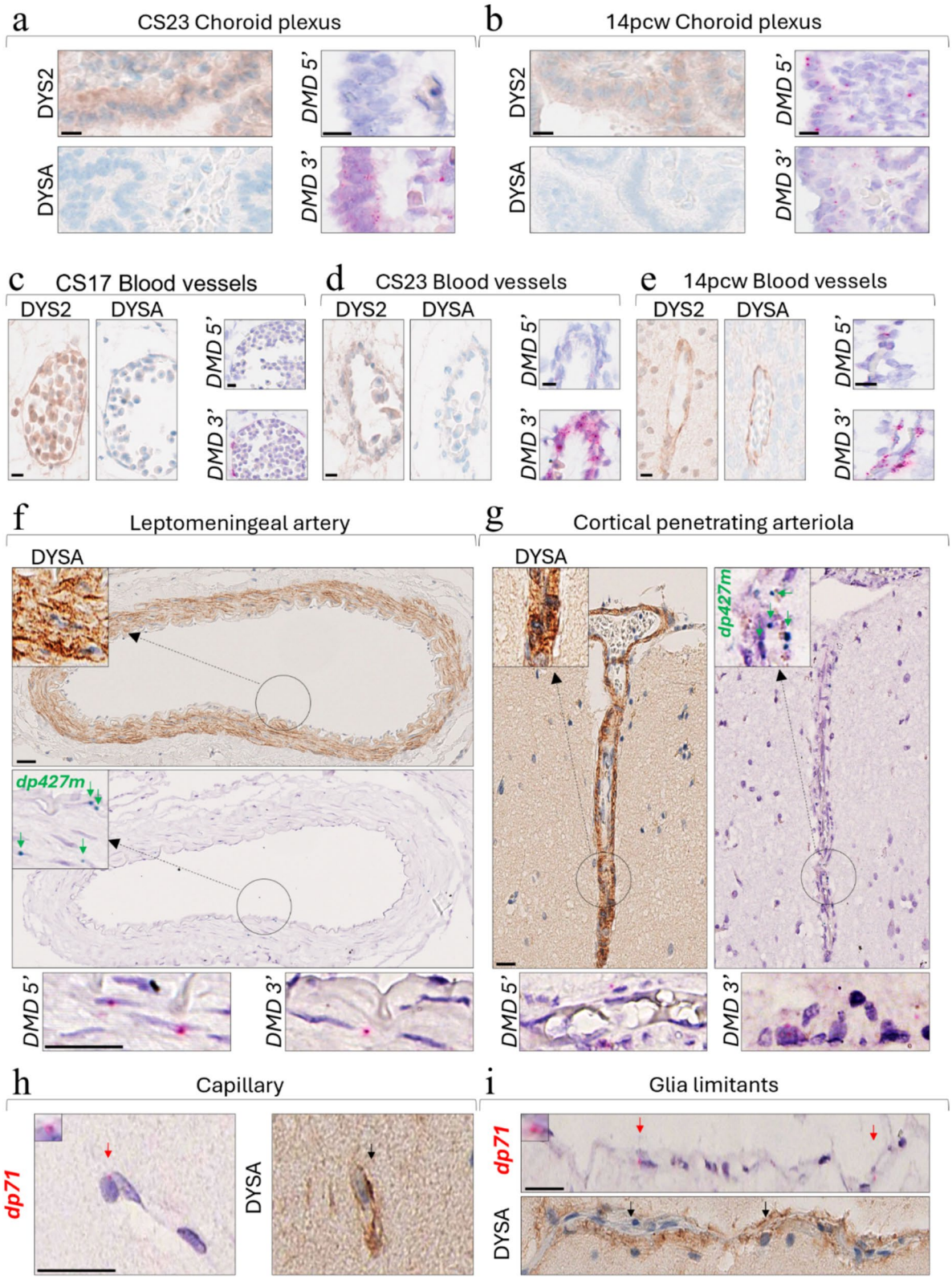

Fig. 13 (See legend on previous page.)

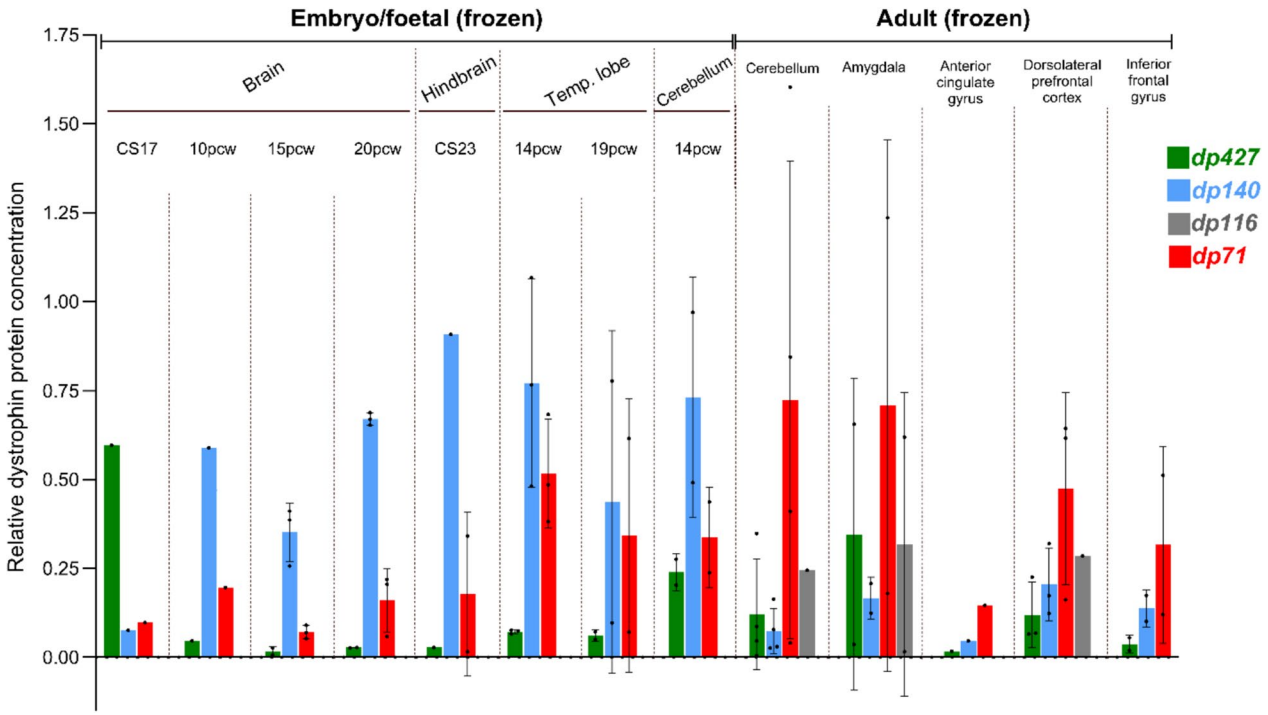

Fig. 14 Detection of dystrophin in developing and adult human brain regions by capillary western blot. Relative dystrophin protein concentration (Dp427) in brain/brain regions from embryos (n = 2), foetuses (n = 15) and adults (n = 12) detected by the C-terminal antibody Ab154168. *Pcw* postconceptional weeks, *CS* Carnegie stage

and adult human brain [4, 12], we found this isoform highly expressed (RT-qPCR) in the embryonic and foetal brains and still detectable, though at low levels, in some adult brain regions. Interestingly expression of two *dp427p* variants was detected by RNA protection assay by Holder et al. [4] in adult brains. It is conceivable that the differences observed across studies are due to different techniques used or probes targeting different *dp427p* variants. It should also be noted that *dp427p2* is believed to translate a truncated protein, which may or may not have a function, whereas *dp427p1* translates a full length protein [4, 42].

Like *dp427p,* expression of *dp427m* was high during development, but more variable in the adult brain. Most of the transcripts were expressed in the leptomeningeal and/or the parenchymal blood vessels within the smooth muscles. Unexpectedly, as not previously reported, consistent expression of *dp427m*, though at very low-levels, was observed in neurons and oligodendroglial-like cells across different brain regions.

Dp140 was highly expressed across all brain regions in the embryonic and foetal brain. In the adult brain its expression was significantly downregulated, with sparse to few transcripts noted in the cerebellum (Purkinje cells, granule cells and dentate neurons), hippocampus (dentate granule cells and hilar neurons), amygdala and across all neocortical areas (mostly in pyramidal neurons). Similarly, prior investigations reported a developmental regulation of *dp140* characterised by high transcripts expression in foetal samples which remain stable in cerebral cortex and cerebellum in adults [12]. Our findings also support the hypothesis that the *dp140* isoform is pivotal during development and persists in the adult brain in areas likely to undergo adult neurogenesis, such as the subgranular zone in the dentate gyrus of the hippocampus, as previously proposed [12, 38].

In keeping with earlier findings, *dp71/dp40* expression was consistently high during development and persisted in the adult brains across all regions. Transcripts were identified within neurons, parenchymal capillary walls (likely astroglia), and the glia limitans. Low-to-moderate *dp40* expression was noted throughout development and persisted in the adult brain.

In addition, we have demonstrated for the first time co-expression of two different *DMD* isoforms within the same neuron by duplex Basescope assays. This can be observed from the early developmental stages to adulthood across all anatomical brain regions. However, neurons co-expressing *DMD* isoforms represent less than approximately 2% of the total neuronal population.

It should be noted that gene co-expression studies suggest distinct roles for *dp427*, *dp140* and *dp71*-related

dystrophin signalling in the brain. Our study has also shown that the granule cells of the dentate gyrus in the hippocampus, neurons in the pontine nuclei, and the cerebellar granular cells displayed the most diversity in *DMD* isoform expression.

With regard to protein expression our western blot results showing good agreement with the RT-qPCR data, confirmed for the first time that the dp140 protein was the predominant isoform expressed in embryonic brains, whereas dp71 was more abundant in adult brains.

Dp427 was consistently expressed throughout development and in adult life. Unexpectedly, we detected expression of dp116 both at the transcript and protein level in developing and adult brains, mainly in the cerebellum and dorsolateral prefrontal cortex. This indicates that dp116 expression may not be restricted to the Schwann cells as previously suggested [12]. We also showed by RT-qPCR that *dp260-1* is the only *DMD* isoform not expressed in the CNS.

Substantial presence of dystrophin in the brain was further supported by immunolabeling with the DYSA antibody showing dystrophin expression mainly in the somata and proximal dendrites of a diverse population of neurons, including pyramidal cells in the neocortex and hippocampus, granule cells of the dentate gyrus, Purkinje cells, granule cells and dentate neurons in the cerebellum, and neuronal populations in the deep grey nuclei (basal ganglia and thalamus), brain stem and cervical cord (anterior horn cells).

The use of duplex RNAscope assays allowed us to study cellular coexpression of dystrophin and markers of GABAergic (*GAD1)* and glutamatergic (*SLC17A7)* neurons circumventing limitations of other approaches (e.g. poor reactivity of dystrophin antibodies in FFPE brain sections and lack of isoform-specific dystrophin antibodies), and to demonstrate dystrophin expression in both *GAD1*+ inhibitory interneurons and *SLC17A7*+ excitatory neurons in all neocortical regions, cerebellum and the hippocampus. Furthermore, the extensive co-expression of *GAD1*+ and *DMD* 3′ transcripts observed in the 14pcw developing Purkinje layer suggest that dystrophin might play a crucial role in the cerebellar GABAergic circuitry maturation. Our data also demonstrate a switch from these isoforms to full length dystrophin in adult GAD1+ Purkinje neurons, as indicated by significant expression of *DMD* 5′ transcripts in these neurons. Transient expression of non-full length isoforms in GAD1+ Purkinje neurons is interesting, as *Dp71*-null mice display alterated glutamatergic transmission and cognitive deficits [28], and is consistent with a realatively early onset of developmental defects leading to at least some of the neural deficit observed in DMD patients.

The dystrophin isoform brain localisation reported here provides an important underpinning to better understand the common brain involvement in DMD patients.

Notably, although impacted by limitations mainly related to small sample size, clinical studies showed that proximal and distal DMD mutations are linked to type and severity of different brain co-morbidities [13, 43, 44].

In most patients, distal mutations are associated with more severe intellectual disability mainly linked to the loss of *dp140* and *dp71* [13, 45–47] leading to reduced intelligent quotients and working memory index scores [13] along with poorer academic performances [48].

In contrast, proximal mutations affecting only *dp427* have been associated with neuropsychiatric manifestations ranging from an increased startle response, indicative of enhanced anxiety and authistic spectrum and attention deficit hyperactivity disorders, without significantly affecting intelligence quotient [13, 14, 49].

DMD has always been regarded as a primary muscle disease. There are no reports of dystrophin expression within the motor systems of the central nervous system in mouse models or in human tissues to date, to the best of our knowledge. In this context, our finding that *DMD* transcripts (5′ and 3′) were present in the upper motor neurons of the primary motor cortex, and the anterior horn cells in the spinal cord in the adult brain is interesting, as it suggests a role for dystrophin in synaptic signalling in the upper and lower motor neurons. An absence of one or more isoforms in these motor neurons could contribute to the motor deficits seen in DMD.

Our findings on dystrophin expression in brain blood vessels both during development and in adults are consistent with its previously reported expression in muscle blood vessels; interestingly, impaired angiogenesis was observed in muscle of DMD patients and animal models [50–53]. In addition, consistent with a possible vascular phenotype in DMD patient brain is the reduced perfusion observed in the *mdx* mouse brain [54] and impaired cerebral blood flow in DMD patients demonstrated by magnetic resonance imaging studies [55].

We are aware that our study has a number of limitations. Although we presented a temporally resolved dystrophin expression profile, the numbers of human brain samples in each age-group are very small. Information regarding dystrophin expression in the crucial post-natal and paediatric age-group is missing, because pathology-free brains for assessment in this age group were not available. Inherent variability (biological and technical) within and in between samples

must be taken in to account while interpreting the data. In particular, accurate quantification of the in situ hybridisation signal was hampered by the sheer number and complexity of neuronal and glial elements in tissue sections, further compounded by the lack of clear cell boundaries, and often saturation of the particulate chromogenic signal within individual neurons.

Given the rapid advancement of single-cell and single-nucleus RNA sequencing technologies as well as single cell proteomics, it will eventually be possible to unravel the complexity of the brain dystrophin cellulome/proteome/interactome. However, validation of such findings in human pathology-free brains as well as DMD brains will remain challenging due to the aforementioned reasons.

Conclusions

In summary, we have shown that *DMD* and dystrophin isoforms are abundantly expressed in the human brain across the lifespan and are developmentally regulated, and localised them at single-cell resolution. We have demonstrated for the first time co-expression of different *DMD* isoforms across several key brain areas in the developing and adult human brain at the regional and single-cell level.

We also have shown for the first time ubiquitous expression of dystrophin within different glutamatergic neuronal populations in the developing human brain. This finding should prompt future studies investigating the molecular pathology of dystrophin signalling at the neuronal excitatory synapse. In addition, we have provided novel information on *DMD* gene expression in GABAergic and glutamatergic neuronal populations in the human brain. The granular localisation of dystrophin reported here will also underpin therapeutic developments aimed at restoring dystrophin functionality in the CNS, hence reducing the burden of brain comorbidities and improving the quality of life of DMD patients.

Supplementary Information

The online version contains supplementary material available at https://doi.org/10.1186/s40478-025-01996-z.

Additional file 1.

Acknowledgements
The authors are thankful to Sarepta Therapeutics for providing financial support for developing this research project. The authors would also like to thank the NIHR GOSH biomedical research centre (BRC) for providing part of the facilities and equipment. We thank the Human Developmental Biology Resource (http://hdbr.org), Edinburgh Brain Bank and BRAIN UK (https://brain-uk.org) for providing human tissue. Special thanks are extended also to the General Department of Health Affairs at Princess Nourah bint Abdulrahman University and Saudi Arabian Cultural Bureau and Ministry of Education (scholarship to RA). We would also like to acknowledge Dr. Karl Frontzek and Professor Maria Thom for providing annotations for a set of brain images and Professor Jennifer Morgan and Dr. Federica Montanaro for their support and useful discussions throughout the project.

Author contributions
FC, DC, RA, SS and AA carried out the experiments. FC, DC, SS and RP performed semi-quantitative scoring. RP and FC designed the analysis. FC performed data analysis and wrote the manuscript. FC, PF, RP and JM edited the manuscript. FM, PF and RP contributed to the conception of the project. FM obtained funding.

Funding
Sarepta Therapeutics Grant 557462.

Availability of data and materials
No datasets were generated or analysed during the current study.

Declarations

Ethics approval and consent to participate
Human tissue procedures were conducted in accordance with the regulations with informed consent in accordance with the UK Human Tissue Act 2006 for study participation under ethical approval (NRES Committee London—Fulham, UK; REC: 18/LO/0822). The human embryonic and foetal material was provided by the Joint MRC/Wellcome Trust (Grants MR/006237/1, MR/X008304/1 and 226202/Z/22/Z) Human Developmental Biology Resource (https://www.hdbr.org). Adult human brains were selected and procured from the Edinburgh Brain Bank (Ethic Ref 20/PR/0582). Tissue samples were obtained from the Edinburgh Brain Bank (EBB) and BRAIN UK, which is supported by Brain Tumour Research and has been established with the support of the British Neuropathological Society and the Medical Research Council.

Consent for publication
Not applicable.

Competing interests
As COI, FM is an investigator in Sarepta, Genethon, Roche clinical trials. He is the PI of the Sarepta grant supporting this work (funding to UCL), and has participated to advisory boards and/or symposia for Sarepta, Roche, Dyne therapeutics, Wave and Entrada.

Author details
[1]The Dubowitz Neuromuscular Centre, Developmental Neurosciences Programme, Great Ormond Street Institute of Child Health, University College London, 30 Guilford Street, London WC1N 1EH, UK. [2]National Institute for Health Research, Great Ormond Street Institute of Child Health Biomedical Research Centre, University College London, London, UK. [3]Dubowitz Neuromuscular Centre, Division of Neuropathology, UCL Queen Square Institute of Neurology, Queen Square, London, UK. [4]Developmental Biology and Cancer Department, UCL Great Ormond Street Institute of Child Health, London WC1N 1EH, UK. [5]Research Department, Natural and Health Science Research Centre, Princess Nourah Bint Abdulrahman University, Riyadh, Saudi Arabia. [6]Sarepta Therapeutics Lnc., Cambridge, MA, USA.

Received: 27 December 2024 Accepted: 2 April 2025
Published online: 21 May 2025

References

1. Muntoni F, Torelli S, Ferlini A (2003) Dystrophin and mutations: one gene, several proteins, multiple phenotypes. Lancet Neurol 2(12):731–740
2. Feener CA, Koenig M, Kunkel LM (1989) Alternative splicing of human dystrophin mRNA generates isoforms at the carboxy terminus. Nature 338(6215):509–511

3. Hildyard JCW, Piercy RJ (2023) When size really matters: the eccentricities of dystrophin transcription and the hazards of quantifying mrna from very long genes. Biomedicines 11(7):2082
4. Holder E, Maeda M, Bies RD (1996) Expression and regulation of the dystrophin Purkinje promoter in human skeletal muscle, heart, and brain. Hum Genet 97(2):232–239
5. Gorecki DC, Monaco AP, Derry JM, Walker AP, Barnard EA, Barnard PJ (1992) Expression of four alternative dystrophin transcripts in brain regions regulated by different promoters. Hum Mol Genet 1(7):505–510
6. Yiu EM, Kornberg AJ (2015) Duchenne muscular dystrophy. J Paediatr Child Health 51(8):759–764
7. Lo Mauro A, Aliverti A (2016) Physiology of respiratory disturbances in muscular dystrophies. Breathe (Sheff) 12(4):318–327
8. Gumerson JD, Michele DE (2011) The dystrophin–glycoprotein complex in the prevention of muscle damage. J Biomed Biotechnol 2011:210797
9. Gao QQ, McNally EM (2015) The dystrophin complex: structure, function, and implications for therapy. Compr Physiol 5(3):1223–1239
10. McArdle A, Edwards RH, Jackson MJ (1995) How does dystrophin deficiency lead to muscle degeneration? Evidence from the mdx mouse. Neuromuscul Disord 5(6):445–456
11. Nudel U, Zuk D, Einat P, Zeelon E, Levy Z, Neuman S, Yaffe D (1989) Duchenne muscular dystrophy gene product is not identical in muscle and brain. Nature 337(6202):76–78
12. Doorenweerd N, Mahfouz A, van Putten M, Kaliyaperumal R, t'Hoen PA, Hendriksen JGM, Aartsma-Rus AM, Verschuuren J, Niks EH, Reinders MJT, Kan HE, Lelieveldt BPF (2017) Timing and localization of human dystrophin isoform expression provide insights into the cognitive phenotype of Duchenne muscular dystrophy. Sci Rep 7(1):12575
13. Ricotti V, Mandy WP, Scoto M, Pane M, Deconinck N, Messina S, Mercuri E, Skuse DH, Muntoni F (2016) Neurodevelopmental, emotional, and behavioural problems in Duchenne muscular dystrophy in relation to underlying dystrophin gene mutations. Dev Med Child Neurol 58(1):77–84
14. Maresh K, Papageorgiou A, Ridout D, Harrison NA, Mandy W, Skuse D, Muntoni F (2023) Startle responses in Duchenne muscular dystrophy: a novel biomarker of brain dystrophin deficiency. Brain 146(1):252–265
15. Taylor PJ, Betts GA, Maroulis S, Gilissen C, Pedersen RL, Mowat DR, Johnston HM, Buckley MF (2010) Dystrophin gene mutation location and the risk of cognitive impairment in Duchenne muscular dystrophy. PLoS ONE 5(1):e8803
16. Felisari G, Martinelli Boneschi F, Bardoni A, Sironi M, Comi GP, Robotti M, Turconi AC, Lai M, Corrao G, Bresolin N (2000) Loss of Dp140 dystrophin isoform and intellectual impairment in Duchenne dystrophy. Neurology 55(4):559–564
17. Doorenweerd N (2020) Combining genetics, neuropsychology and neuroimaging to improve understanding of brain involvement in Duchenne muscular dystrophy—a narrative review. Neuromuscul Disord 30(6):437–442
18. Darmahkasih AJ, Rybalsky I, Tian C, Shellenbarger KC, Horn PS, Lambert JT, Wong BL (2020) Neurodevelopmental, behavioral, and emotional symptoms common in Duchenne muscular dystrophy. Muscle Nerve 61(4):466–474
19. Lee AJ, Buckingham ET, Kauer AJ, Mathews KD (2018) Descriptive phenotype of obsessive compulsive symptoms in males with duchenne muscular dystrophy. J Child Neurol 33(9):572–579
20. Astrea G, Pecini C, Gasperini F, Brisca G, Scutifero M, Bruno C, Santorelli FM, Cioni G, Politano L, Chilosi AM, Battini R (2015) Reading impairment in Duchenne muscular dystrophy: a pilot study to investigate similarities and differences with developmental dyslexia. Res Dev Disabil 45–46:168–177
21. Brunig I, Suter A, Knuesel I, Luscher B, Fritschy JM (2002) GABAergic terminals are required for postsynaptic clustering of dystrophin but not of GABA(A) receptors and gephyrin. J Neurosci 22(12):4805–4813
22. Bagdatlioglu E, Porcari P, Greally E, Blamire AM, Straub VW (2020) Cognitive impairment appears progressive in the mdx mouse. Neuromuscul Disord 30(5):368–388
23. Suzuki Y, Higuchi S, Aida I, Nakajima T, Nakada T (2017) Abnormal distribution of GABA(A) receptors in brain of duchenne muscular dystrophy patients. Muscle Nerve 55(4):591–595
24. Hashimoto Y, Kuniishi H, Sakai K, Fukushima Y, Du X, Yamashiro K, Hori K, Imamura M, Hoshino M, Yamada M, Araki T, Sakagami H, Takeda S, Itaka K, Ichinohe N, Muntoni F, Sekiguchi M, Aoki Y (2022) Brain Dp140 alters glutamatergic transmission and social behaviour in the mdx52 mouse model of Duchenne muscular dystrophy. Prog Neurobiol 216:102288
25. Araki E, Nakamura K, Nakao K, Kameya S, Kobayashi O, Nonaka I, Kobayashi T, Katsuki M (1997) Targeted disruption of exon 52 in the mouse dystrophin gene induced muscle degeneration similar to that observed in Duchenne muscular dystrophy. Biochem Biophys Res Commun 238(2):492–497
26. Doorenweerd N, Straathof CS, Dumas EM, Spitali P, Ginjaar IB, Wokke BH, Schrans DG, van den Bergen JC, van Zwet EW, Webb A, van Buchem MA, Verschuuren JJ, Hendriksen JG, Niks EH, Kan HE (2014) Reduced cerebral gray matter and altered white matter in boys with Duchenne muscular dystrophy. Ann Neurol 76(3):403–411
27. Cheng B, Xu H, Zhou H, Guo Y, Roberts N, Li N, Hu X, Chen X, Xu K, Lan Y, Ma X, Cai X, Guo Y (2023) Connectomic disturbances in Duchenne muscular dystrophy with mild cognitive impairment. Cereb Cortex 33(11):6785–6791
28. Daoud F, Angeard N, Demerre B, Martie I, Benyaou R, Leturcq F, Cossee M, Deburgrave N, Saillour Y, Tuffery S, Urtizberea A, Toutain A, Echenne B, Frischman M, Mayer M, Desguerre I, Estournet B, Reveillere C, Penisson B, Cuisset JM, Kaplan JC, Heron D, Rivier F, Chelly J (2009) Analysis of Dp71 contribution in the severity of mental retardation through comparison of Duchenne and Becker patients differing by mutation consequences on Dp71 expression. Hum Mol Genet 18(20):3779–3794
29. Helleringer R, Le Verger D, Li X, Izabelle C, Chaussenot R, Belmaati-Cherkaoui M, Dammak R, Decottignies P, Daniel H, Galante M, Vaillend C (2018) Cerebellar synapse properties and cerebellum-dependent motor and non-motor performance in Dp71-null mice. Dis Model Mech 11(7):dmm033258
30. Chesshyre M, Ridout D, Hashimoto Y, Ookubo Y, Torelli S, Maresh K, Ricotti V, Abbott L, Gupta VA, Main M, Ferrari G, Kowala A, Lin YY, Tedesco FS, Scoto M, Baranello G, Manzur A, Aoki Y, Muntoni F (2022) Investigating the role of dystrophin isoform deficiency in motor function in Duchenne muscular dystrophy. J Cachexia Sarcopenia Muscle 13(2):1360–1372
31. Hawrylycz MJ, Lein ES, Guillozet-Bongaarts AL, Shen EH, Ng L, Miller JA, van de Lagemaat LN, Smith KA, Ebbert A, Riley ZL, Abajian C, Beckmann CF, Bernard A, Bertagnolli D, Boe AF, Cartagena PM, Chakravarty MM, Chapin M, Chong J, Dalley RA, David Daly B, Dang C, Datta S, Dee N, Dolbeare TA, Faber V, Feng D, Fowler DR, Goldy J, Gregor BW, Haradon Z, Haynor DR, Hohmann JG, Horvath S, Howard RE, Jeromin A, Jochim JM, Kinnunen M, Lau C, Lazarz ET, Lee C, Lemon TA, Li L, Li Y, Morris JA, Overly CC, Parker PD, Parry SE, Reding M, Royall JJ, Schulkin J, Sequeira PA, Slaughterbeck CR, Smith SC, Sodt AJ, Sunkin SM, Swanson BE, Vawter MP, Williams D, Wohnoutka P, Zielke HR, Geschwind DH, Hof PR, Smith SM, Koch C, Grant SGN, Jones AR (2012) An anatomically comprehensive atlas of the adult human brain transcriptome. Nature 489(7416):391–399
32. Miller JA, Ding SL, Sunkin SM, Smith KA, Ng L, Szafer A, Ebbert A, Riley ZL, Royall JJ, Aiona K, Arnold JM, Bennet C, Bertagnolli D, Brouner K, Butler S, Caldejon S, Carey A, Cuhaciyan C, Dalley RA, Dee N, Dolbeare TA, Facer BA, Feng D, Fliss TP, Gee G, Goldy J, Gourley L, Gregor BW, Gu G, Howard RE, Jochim JM, Kuan CL, Lau C, Lee CK, Lee F, Lemon TA, Lesnar P, McMurray B, Mastan N, Mosqueda N, Naluai-Cecchini T, Ngo NK, Nyhus J, Oldre A, Olson E, Parente J, Parker PD, Parry SE, Stevens A, Pletikos M, Reding M, Roll K, Sandman D, Sarreal M, Shapouri S, Shapovalova NV, Shen EH, Sjoquist N, Slaughterbeck CR, Smith M, Sodt AJ, Williams D, Zollei L, Fischl B, Gerstein MB, Geschwind DH, Glass IA, Hawrylycz MJ, Hevner RF, Huang H, Jones AR, Knowles JA, Levitt P, Phillips JW, Sestan N, Wohnoutka P, Dang C, Bernard A, Hohmann JG, Lein ES (2014) Transcriptional landscape of the prenatal human brain. Nature 508(7495):199–206
33. Nicoll JAR, Bloom T, Clarke A, Boche D, Hilton D (2022) BRAIN UK: accessing NHS tissue archives for neuroscience research. Neuropathol Appl Neurobiol 48(2):e12766
34. Krafft AE, Duncan BW, Bijwaard KE, Taubenberger JK, Lichy JH (1997) Optimization of the isolation and amplification of RNA from formalin-fixed, paraffin-embedded tissue: the armed forces institute of pathology experience and literature review. Mol Diagn 2(3):217–230
35. Li J, Smyth P, Cahill S, Denning K, Flavin R, Aherne S, Pirotta M, Guenther SM, O'Leary JJ, Sheils O (2008) Improved RNA quality and TaqMan Pre-amplification method (PreAmp) to enhance expression analysis from formalin fixed paraffin embedded (FFPE) materials. BMC Biotechnol 8:10

36. Zeka F, Vanderheyden K, De Smet E, Cuvelier CA, Mestdagh P, Vandesompele J (2016) Straightforward and sensitive RT-qPCR based gene expression analysis of FFPE samples. Sci Rep 6:21418
37. Kong H, Zhu M, Cui F, Wang S, Gao X, Lu S, Wu Y, Zhu H (2014) Quantitative assessment of short amplicons in FFPE-derived long-chain RNA. Sci Rep 4:7246
38. Hildyard JCW, Crawford AH, Rawson F, Riddell DO, Harron RCM, Piercy RJ (2020) Single-transcript multiplex in situ hybridisation reveals unique patterns of dystrophin isoform expression in the developing mammalian embryo. Wellcome Open Res 5:76
39. Son AI, Mohammad S, Sasaki T, Ishii S, Yamashita S, Hashimoto-Torii K, Torii M (2020) Dual role of Rbpj in the maintenance of neural progenitor cells and neuronal migration in cortical development. Cereb Cortex 30(12):6444–6457
40. McClenahan FK, Sharma H, Shan X, Eyermann C, Colognato H (2016) Dystroglycan suppresses notch to regulate stem cell niche structure and function in the developing postnatal subventricular zone. Dev Cell 38(5):548–566
41. Crawford AH, Hildyard JCW, Rushing SAM, Wells DJ, Diez-Leon M, Piercy RJ (2022) Validation of DE50-MD dogs as a model for the brain phenotype of Duchenne muscular dystrophy. Dis Model Mech 15(3):dmm049291
42. Garcia-Cruz C, Aragon J, Lourdel S, Annan A, Roger JE, Montanez C, Vaillend C (2023) Tissue- and cell-specific whole-transcriptome meta-analysis from brain and retina reveals differential expression of dystrophin complexes and new dystrophin spliced isoforms. Hum Mol Genet 32(4):659–676
43. Pascual-Morena C, Cavero-Redondo I, Martinez-Vizcaino V, Sequi-Dominguez I, Fernandez-Bravo-Rodrigo J, Jimenez-Lopez E (2023) Dystrophin genotype and risk of neuropsychiatric disorders in dystrophinopathies: a systematic review and meta-analysis. J Neuromuscul Dis 10(2):159–172
44. Milic Rasic V, Vojinovic D, Pesovic J, Mijalkovic G, Lukic V, Mladenovic J, Kosac A, Novakovic I, Maksimovic N, Romac S, Todorovic S, Savic Pavicevic D (2014) Intellectual ability in the duchenne muscular dystrophy and dystrophin gene mutation location. Balkan J Med Genet 17(2):25–35
45. Bardoni A, Felisari G, Sironi M, Comi G, Lai M, Robotti M, Bresolin N (2000) Loss of Dp140 regulatory sequences is associated with cognitive impairment in dystrophinopathies. Neuromuscul Disord 10(3):194–199
46. Moizard MP, Billard C, Toutain A, Berret F, Marmin N, Moraine C (1998) Are Dp71 and Dp140 brain dystrophin isoforms related to cognitive impairment in Duchenne muscular dystrophy? Am J Med Genet 80(1):32–41
47. Chamova T, Guergueltcheva V, Raycheva M, Todorov T, Genova J, Bichev S, Bojinova V, Mitev V, Tournev I, Todorova A (2013) Association between loss of dp140 and cognitive impairment in duchenne and becker dystrophies. Balkan J Med Genet 16(1):21–30
48. Fee RJ, Montes J, Stewart JL, Hinton VJ (2018) Executive skills and academic achievement in the dystrophinopathies. J Int Neuropsychol Soc 24(9):928–938
49. Pane M, Lombardo ME, Alfieri P, D'Amico A, Bianco F, Vasco G, Piccini G, Mallardi M, Romeo DM, Ricotti V, Ferlini A, Gualandi F, Vicari S, Bertini E, Berardinelli A, Mercuri E (2012) Attention deficit hyperactivity disorder and cognitive function in Duchenne muscular dystrophy: phenotype-genotype correlation. J Pediatr 161(4):705-9e1
50. Miike T, Sugino S, Ohtani Y, Taku K, Yoshioka K (1987) Vascular endothelial cell injury and platelet embolism in Duchenne muscular dystrophy at the preclinical stage. J Neurol Sci 82(1–3):67–80
51. Thomas GD (2013) Functional muscle ischemia in Duchenne and Becker muscular dystrophy. Front Physiol 4:381
52. Kodippili K, Thorne PK, Laughlin MH, Duan D (2021) Dystrophin deficiency impairs vascular structure and function in the canine model of Duchenne muscular dystrophy. J Pathol 254(5):589–605
53. Loufrani L, Dubroca C, You D, Li Z, Levy B, Paulin D, Henrion D (2004) Absence of dystrophin in mice reduces NO-dependent vascular function and vascular density: total recovery after a treatment with the aminoglycoside gentamicin. Arterioscler Thromb Vasc Biol 24(4):671–676
54. Goodnough CL, Gao Y, Li X, Qutaish MQ, Goodnough LH, Molter J, Wilson D, Flask CA, Yu X (2014) Lack of dystrophin results in abnormal cerebral diffusion and perfusion in vivo. Neuroimage 102(2):809–816
55. Doorenweerd N, Dumas EM, Ghariq E, Schmid S, Straathof CS, Roest AA, Wokke BH, van Zwet EW, Webb AG, Hendriksen JG, van Buchem MA, Verschuuren JJ, Asllani I, Niks EH, van Osch MJ, Kan HE (2017) Decreased cerebral perfusion in Duchenne muscular dystrophy patients. Neuromuscul Disord 27(1):29–37

Publisher's Note